Therapeutic inhibition of keratinocyte TRPV3 sensory channel by local anesthetic dyclonine

Qiang Liu, Jin Wang, Xin Wei, Juan Hu, Conghui Ping, Yue Gao, Chang Xie, Peiyu Wang, Peng Cao, Zhengyu Cao, et al.

Therapeutic inhibition of keratinocyte TRPV3 sensory channel by local anesthetic dyclonine

Qiang Liu[1,6], Jin Wang[2,6], Xin Wei[1], Juan Hu[1], Conghui Ping[1], Yue Gao[1], Chang Xie[1], Peiyu Wang[1], Peng Cao[3], Zhengyu Cao[4], Ye Yu[2], Dongdong Li[5], Jing Yao[1]✉

[1] State Key Laboratory of Virology, Hubei Key Laboratory of Cell Homeostasis, College of Life Sciences, Frontier Science Center for Immunology and Metabolism, Wuhan University, Wuhan, Hubei 430072, China

[2] School of Basic Medicine and Clinical Pharmacy, China Pharmaceutical University, Nanjing, Jiangsu 211198, China

[3] Hospital of Integrated Traditional Chinese and Western Medicine, Nanjing University of Chinese Medicine, Nanjing 210023

[4] State Key Laboratory of Natural Medicines and Jiangsu Provincial Key Laboratory for TCM Evaluation and Translational Development, School of Traditional Chinese Pharmacy, China Pharmaceutical University, Nanjing Jiangsu 211198, China

[5] Sorbonne Université, Institute of Biology Paris Seine, Neuroscience Paris Seine, CNRS UMR8246, INSERM U1130, Paris 75005, France

[6] These authors contributed equally to this work.

Running title: Inhibition of TRPV3 channels by dyclonine

Keywords: TRPV3, Dyclonine, Cell death, Pruritus, Skin inflammation

✉ Address correspondence to:
Dr. Jing Yao
State Key Laboratory of Virology,
Hubei Key Laboratory of Cell Homeostasis,
College of Life Sciences,
Frontier Science Center for Immunology and Metabolism,
Wuhan University,
Wuhan, Hubei 430072, China
Phone: 86-27-68752148
Email: jyao@whu.edu.cn

Abstract

The multimodal sensory channel transient receptor potential vanilloid-3 (TRPV3) is expressed in epidermal keratinocytes and implicated in chronic pruritus, allergy, and inflammation-related skin disorders. Gain-of-function mutations of TRPV3 cause hair growth disorders in mice and Olmsted Syndrome in human. Nevertheless, whether and how TRPV3 could be therapeutically targeted remains to be elucidated. We here report that mouse and human TRPV3 channel is targeted by the clinical medication dyclonine that exerts a potent inhibitory effect. Accordingly, dyclonine rescued cell death caused by gain-of-function TRPV3 mutations and suppressed pruritus symptoms in vivo in mouse model. At the single-channel level, dyclonine inhibited TRPV3 open probability but not the unitary conductance. By molecular simulations and mutagenesis, we further uncovered key residues in TRPV3 pore region that could toggle the inhibitory efficiency of dyclonine. The functional and mechanistic insights obtained on dyclonine-TRPV3 interaction will help to conceive updated therapeutics for skin inflammation.

Introduction

Transient receptor potential (TRP) channels belong to a family of calcium-permeable and nonselective cation channels, essential for body sensory processing and local inflammatory development (Clapham, 2003). As a polymodal cellular sensor, TRPV3 channel is abundantly expressed in skin keratinocytes (Chung, Lee, Mizuno, Suzuki, & Caterina, 2004c; Peier et al., 2002; Xu et al., 2002) and in cells surrounding the hair follicles (Cheng et al., 2010). TRPV3 integrates a wide spectrum of physical and chemical stimuli (Luo & Hu, 2014). TRPV3 is sensitive to innocuous temperatures above 30-33 °C and exhibits an increased response at noxious temperature (Chung, Guler, & Caterina, 2005; Xu et al., 2002). Natural plant products such as camphor (Moqrich et al., 2005), carvacrol, eugenol, thymol (Xu, Delling, Jun, & Clapham, 2006), and the pharmacological compound 2-aminoethoxydiphenyl borate (2-APB) (Chung, Lee, Mizuno, Suzuki, & Caterina, 2004b; Colton & Zhu, 2007) also activate TRPV3. In addition, TRPV3 is directly activated by acidic pH from cytoplasmic side (Gao et al., 2016).

Mounting evidence implicates TRPV3 channel in cutaneous sensation including thermal sensation (Chung et al., 2004c), nociception (S. M. Huang et al., 2008), and itch (Yamamoto-Kasai et al., 2012). They also participate in the maintenance of skin barrier, hair growth (Cheng et al., 2010) and wound healing (Aijima et al., 2015; Yamada et al., 2010). Recently, the dysfunction of TRPV3 channels has come to the fore as a key regulator of physio- and pathological responses of skin (Ho & Lee,

2015). In rodents, the Gly573Ser substitution in TRPV3 renders the channel spontaneously active and caused a hairless phenotype in DS-Nh mice and WBN/Kob-Ht rats (Asakawa et al., 2006). DS-Nh mice also develop severe scratching behavior and pruritic dermatitis. TRPV3 dysfunction caused by genetic gain-of-function mutations or pharmaceutical activation has been linked to human skin diseases including genodermatosis known as Olmsted syndrome (Agarwala, George, Pramanik, & McGrath, 2016; Lin et al., 2012) and erythromelalgia (Duchatelet et al., 2014). Furthermore, TRPV3-deficient mice give rise to phenotypes of curly whiskers and wavy hair coat (Cheng et al., 2010). Conversely, hyperactive TRPV3 channels expressed in human outer root sheath keratinocytes inhibit hair growth (Borbiro et al., 2011). While being implicated in a variety of skin disorders, whether and how TRPV3 could be therapeutically targeted remains to be elucidated. It is thus desirable to identify and understand clinical medications that can potentially target TRPV3 channels.

As a clinical anesthetic, dyclonine is characterized by rapid onset of effect, lack of systemic toxicity, and a low index of sensitization (Florestano & Bahler, 1956). Its topical application (0.5% or 1% dyclonine hydrochloride contained in the topical solution, i.e., ~30.7 mM at a dose of 1%, according to the United States Pharmacopeia) rapidly relieves itching and pain in patients, by ameliorating inflamed, excoriated and broken lesions on mucous membranes and skin (Morginson et al., 1956). Accordingly, dyclonine is used to anesthetize mucous membranes prior to endoscopy (Formaker, Mott, & Frank, 1998). The clinical scenario targeted by dyclonine treatment echoes

the pathological aspects of TRPV3-related skin disorders, suggesting that the therapeutic effects of dyclonine might involve its interaction with TRPV3 sensory channel.

Here, using a multidisciplinary approach combining electrophysiology, genetic engineering and ultrafast local temperature control, we show that mouse and human TRPV3 channel was potently suppressed by dyclonine. It dose-dependently inhibited TRPV3 currents in a voltage-independent manner and rescued cell death caused by TRPV3 gain-of-function mutation. In *vivo*, dyclonine indeed suppressed the itching/scratching behaviors induced by TRPV3 channel agonist carvacrol as evidenced by the TRPV3 knock out (KO) mice. At single-channel level, dyclonine reduced TRPV3 channel open probability without altering the unitary conductance. We also identified molecular residues that were capable of either eliminating or enhancing the inhibitory effect of dyclonine. These data demonstrate the effective inhibition of TRPV3 channel by dyclonine, supplementing a molecular mechanism for its clinical effects and raising its potential to ameliorate TRPV3-associated disorders.

Results

Inhibition of TRPV3 currents by dyclonine

We first examined the effect of dyclonine on TRPV3 activity induced by the TRPV channel agonist 2-APB (100 μM). Whole-cell currents were recorded at a holding potential of -60 mV in HEK 293T cells expressing mouse TRPV3. Because TRPV3 channels exhibit sensitizing properties upon repeated stimulation (Chung, Lee, Mizuno, Suzuki, & Caterina, 2004a), we examined the effect of dyclonine after the response had stabilized following repetitive application of 2-APB (Figure 1A). The presence of 5 μM and 10 μM dyclonine significantly inhibited TRPV3 currents response to 30 ± 2% and 15 ± 3% of control level, respectively. After washing out of dyclonine, 2-APB evoked a similar response to the control level, indicating the blocking effect of dyclonine is reversible (Figure 1A-B). We repeated the experiments with different doses of dyclonine. The dose-response curve indicates that dyclonine inhibited TRPV3 currents in a concentration-dependent manner with an IC_{50} of 3.2 ± 0.24 μM (n = 6, Figure 1C). We further examined the inhibitory effect of dyclonine on TRPV3 activated by varying concentrations of 2-APB (Figure 1D). The dose-response curves to 2-APB were fitted with a Hill equation. The inhibitory effect of dyclonine on TRPV3 activation was consistently observed under all tested 2-APB concentrations (Figure 1E). The corresponding EC_{50} values and Hill coefficients were not changed by the presence of dyclonine (Figure 1E, EC_{50} = 22.93 ± 0.02 μM, n_H = 1.6 ± 0.1 without dyclonine vs. EC_{50} = 22.03 ± 0.86 μM, n_H = 1.7 ± 0.1 with 3 μM dyclonine), as confirmed by the normalized dose-response curves (Figure 1F).

Therefore, dyclonine dose-dependently inhibits the response amplitudes of TRPV3 channel.

TRPV3 channel in physiological conditions has a low level of response to external stimuli, which is augmented during the sensitization process (i.e., repetitive stimulations, Figure 1A). In contrast, excessive up-regulation of TRPV3 activity impairs hair growth and increases the incidence of dermatitis and pruritus in both humans and rodents. To determine whether dyclonine affects the process of TRPV3 sensitization, TRPV3-expressing cells were repeatedly exposed to 100 μM 2-APB without or with 5 μM dyclonine (Figure 1G-H). TRPV3 currents evoked by 2-APB alone took ~8 repetitions to reach full sensitization level (Figure 1I). The presence of dyclonine significantly slowed down this process, requiring ~16 repetitions to reach the current level of full sensitization (Figure 1H-I). As expected, dyclonine also reduced the initial TRPV3 current (31.12 ± 2.86 pA/pF, v.s. 86.43 ± 5.9 pA/pF without dyclonine; $p < 0.001$; $n = 9$ per condition).

As TRPV3 is highly expressed in keratinocytes, we further determined the inhibitory effect of dyclonine in primary mouse epidermal keratinocytes. After stabilizing the channel current by repeated application of 2-APB, we tested the inhibitory effect of 5 μM and 30 μM dyclonine (Figure 1J). On average, TRPV3 currents were reduced to 52 ± 7% and 13 ± 0.01% of control level by 5 μM and 30 μM dyclonine, respectively (Fig. 1K), reaching the similar level of inhibition by the wide-spectrum TRP channel blocker ruthenium red (RR, Figure 1J). From the dose-response curve (Figure 1L), the IC_{50} of dyclonine was assessed to be 5.2 ± 0.71

μM, with a Hill coefficient of n_H = 2.4 ± 0.75 (*n* = 7). Thus, dyclonine effectively suppresses the activity of endogenous TRPV3 channels in mouse keratinocytes.

Dyclonine is a potent inhibitor of TRPV3 channel

Next, we compared the inhibitory effect on TRPV3 of dyclonine to its impact on other TRP channels. TRPV1, TRPV2, TRPM8 and TRPA1 channels were expressed in HEK 293T cells and respectively activated by capsaicin, 2-APB, menthol and Allyl Isothiocyanate (AITC). We observed that 10 μM dyclonine exhibited little inhibition on TRPV1, TRPV2, TRPM8 and TRPA1, but potently inhibited TRPV3 channel (Figure 2A). The corresponding reduction in current amplitude was 2 ± 1% for TRPV1, 6 ± 1% for TRPV2, 9 ± 2% for TRPM8, 5 ± 1% for TRPA1, compared with 87 ± 1% inhibition of TRPV3 current (Figure 2B). By applying a series of dyclonine concentrations, we derived dose-response curves (Figure 2C). The corresponding IC_{50} values of dyclonine for inhibiting TRPV1, TRPV2 TRPM8 and TRPA1 channels (336.3 ± 12.0 μM, 36.5 ± 3.7 μM, 72.4 ± 10.9 μM and 152.35 ± 16.3 μM, respectively) were one or two orders of magnitude higher than that for TRPV3 inhibition (3.2 ± 0.24 μM), indicating that dyclonine represents an effective inhibitor of TRPV3 channel.

Above results were obtained for mouse TRPV3. We further asked whether the inhibitory effect of dyclonine on TRPV3 is consistent across different species. Similarly, we performed whole-cell recordings in HEK 293T cells expressing human TRPV3 and frog TRPV3, respectively. They were activated to a stable level by

repetitive 2-APB stimulation. Addition of dyclonine, indeed, efficiently suppressed the activation of both types of TRPV3 channel (Figure 2D-I). Dose-response curves for dyclonine inhibition yielded an IC_{50} value of 16.2 ± 0.72 μM for hTRPV3 and 12.3 ± 1.6 μM for fTRPV3, respectively. Therefore, the inhibition of TRPV3 by dyclonine is conserved across species.

Inhibition of TRPV3 by dyclonine is voltage-independent

To obtain a complete description of the inhibitory effect of dyclonine, we next investigated its voltage dependence using a stepwise protocol (Figure 3A). We measured membrane currents in TRPV3-expressing HEK 293T cells using a Cs^+-based pipette solution that blocks most outward K^+ channel current but permits measurement of outward conductance mediated by the nonselective TRPV3 channel. A low-concentration 2-APB (40 μM) activated small voltage-dependent currents with steady-state outward rectification, characteristic of TRPV3 currents in heterologous expression systems (Figure 3A). Addition of dyclonine in the extracellular solution significantly diminished TRPV3-mediated outward and inward currents (Figure 3A). By contrast, 10 μM ruthenium red, a broad TRP channel blocker, only inhibited TRPV3-mediated inward currents but enhanced outward currents (Figure 3A), which is consistent with early report (Cheng et al., 2010). Dyclonine inhibition of both inward and outward currents was further confirmed by the I-V curves derived from pooled data (Figure 3B). We found no significant difference inhibition at hyperpolarized voltages versus depolarized voltages, showing the inhibition occurred

independently of the membrane potential (Figure 3C). Together, relative to the wide-spectrum blocker ruthenium red, dyclonine more effectively inhibits TRPV3 channel in a voltage-independent manner.

Inhibition of heat-activated TRPV3 currents by dyclonine

TRPV3 is a thermal sensitive ion channel and has an activation threshold around 30 to 33 °C (Xu et al., 2002). We therefore explored whether the heat-evoked TRPV3 currents can be also inhibited by dyclonine. We employed an ultrafast infrared laser system to control the local temperature near single cells; each temperature jump had a rise time of 1.5 ms and lasted for 100 ms. TRPV3 sensitization of the channel was induced by repeating a same temperature jump from room temperature to ~51 °C (Figure 4A). TRPV3, expressed in HEK 293T cells, steadily responded to temperature jumps ranging from 30 to 51 °C (Figure 4B). After pre-sensitization by repeated temperature jumps from room temperature to 52 °C, application of dyclonine appreciably inhibited TRPV3 thermal currents (Figure 4B-C). The inhibitory effect of dyclonine was fully reversible, as after its washing out the TRPV3 response recovered to the same level as control condition (Figure 4C). To determine the concentration dependence of dyclonine inhibition, TRPV3 currents were evoked by a same temperature jump from room temperature to ~52 °C in the presence of 1, 3, 5, 10, 30, and 50 μM dyclonine (Figure 4D). The IC_{50} of dyclonine on TRPV3 inhibition was assessed to be 14.02 ± 2.5 μM with a Hill coefficient of n_H = 1.9 ± 0.54, according to

the dose-response curve fitting (Figure 4E). These results thus indicate that dyclonine dose-dependently suppresses heat-evoked TRPV3 currents.

Dyclonine inhibited hyperactive TRPV3 mutants and rescued cell death

It has previously been reported that gain-of-function mutations, G573S and G573C, of TRPV3 are constitutively active and their expression causes cell death (Xiao, Tian, Tang, & Zhu, 2008). We firstly examined the effect of dyclonine on the electrophysiological activity of mutants. We transfected the inducible cDNA constructs encoding respectively the GFP-tagged wild-type TRPV3, G573S, or G573 mutant into T-Rex 293 cells and then applied 20 ng/ml doxycycline to induce the gene expression. As illustrated in Figure 5A and B, whole-cell recordings from G573S or G573C expressed in T-Rex 293 cells show that spontaneous currents noticeably appeared when changing the holding potential from 0 mV to -60 mV, and application of 2-APB further increased the channel currents. In each patch, 20 μM RR was applied extracellularly to obtain remaining leak currents. By subtracting leak currents, we found that spontaneous activities from G573S and G573C were reduced by 74 ± 3% (n = 6) and 71 ± 2% (n = 6) by 10 μM dyclonine, respectively (Figure 5C). Also, the presence of dyclonine significantly inhibited 300 μM 2-APB-evoked responses to 10 ± 2% (G573S, n = 6) and 11 ± 1% (G573C, n = 6) of control level (Figure 5D), respectively. As both mutant TRPV3 channels are effectively inhibited by dyclonine, we next explored whether it can rescue the cell death caused by these gain-of-function mutants. Cells expressing G573S or G573S were exposed to different

241 pharmacological drugs (dyclonine, 2-APB, 2-APB and dyclonine, or ruthenium red).
242 Cell death was recognized by the narrow and contracted footprints in bright-field
243 images, and the protein expression meanwhile monitored by GFP fluorescence. As
244 shown in Figure 5E, massive cell death was seen in cells that expressed G573C and
245 G573S TRPV3 mutants but not those expressing the wild type TRPV3. Addition of
246 dyclonine largely prevented the cell death while not causing change in the expression
247 of TRPV3 channels (Figure 5E), indicating that dyclonine decreased the cytotoxicity
248 caused by the gain-of-function mutants. We further performed flow cytometry
249 analysis and observed that the cell death ratio was maintained at low level (4.96 ±
250 0.87%, n = 7) in cells expressing wild-type TRPV3 (Figure 5F). By contrast, the
251 expression of G573S or G573C mutant significantly increased the cell death ratio to
252 45.36 ± 5.79% (n = 7) and 52.74 ± 4.94% (n = 7), that were effectively reduced by
253 dyclonine (50 μM) to 12.45 ± 2.54% (n = 7) and 14.98 ± 4.40% (n = 7), respectively.
254 The cell-protective effect of dyclonine was mirrored by the general TRP channel
255 blocker ruthenium red (Figure 5E-G). As expected, activation of TRPV3 channels
256 with the agonist 2-APB caused significant cell death even in cells expressing
257 wild-type channel and exacerbated the cell death in those expressing the mutant
258 channel G573S or G573C (Figure 5G). Application of dyclonine also reversed the cell
259 death caused by 2-APB activation (9.12 ± 1.42% vs. 43.73 ± 3.46% for wild-type
260 condition, 17.68% ± 5.66% vs. 53.60 ± 5.88% for G573S, and 13.85% ± 2.49% vs.
261 47.91 ± 5.54% for G573C after and before addition of dyclonine). Collectively, these
262 results indicate that dyclonine rescues cell death by inhibiting the excessive activity of

TRPV3 channel.

Dyclonine targets TRPV3 in vivo and ameliorates scratching behavior

TRPV3 is highly expressed in skin keratinocytes, whose hyperactivity causes pruritic dermatitis and scratching behavior. We next examined in vivo the therapeutic effect of dyclonine on TRPV3 hyperactivity-caused scratching behavior in mouse model. Itching-scratching behavior was induced by pharmacological activation of TRPV3 channel by a natural compound carvacrol derived from oregano (Cui, Wang, Wei, & Wang, 2018). The number of scratching bouts was quantified every 5 min (Figure 6A), and also summed over a 30-minute observation period (Figure 6B). Intradermal injection of carvacrol (0.1%, 50 μl) in wild-type TRPV3 mice caused significant increases in the accumulated scratching bouts (137.2 ± 33.9) as compared to the control group receiving normal saline (0.9% NaCl, 3.8 ± 1, n = 6, P < 0.001; Figure 6B). By contrast, intradermal injection of carvacrol (0.1%, 50 μl) did not elicit a remarkable change in the number of scratching bouts in TRPV3$^{-/-}$ mice (Figure 6A-B), supporting that carvacrol caused itching-scratching behavior via TRPV3 activation (Cui et al., 2018). To investigate whether dyclonine could alleviate carvacrol-evoked acute itch, we made an intradermal injection of dyclonine into the mouse neck 30 minutes before the injection of carvacrol into the same site. As illustrated in Figure 6C-D, administration of 50 μl dyclonine at 1, 10 and 50 μM concentrations appreciably reduced the scratching bouts to 130.0 ± 20.3, 82.0 ± 15.0, and 18.0 ± 8.0 from 137.8 ± 18.3 (n = 6), respectively. We also carried out whole-cell recordings in

TRPV3-expressing HEK 293T cells to further confirm the inhibitory effect of dyclonine on TRPV3 currents activated by carvacrol. Similar to that observed with the inhibition of 2-APB-evoked TRPV3 currents (Figure 1A-C), dyclonine also inhibited carvacrol-activated TRPV3 currents in a concentration-dependent manner with IC_{50} = 3.5 ± 0.34 μM following sensitization by repeated application of 300 μM 2-APB (*n* = 8, Figure 6E-F), implying that the itching caused by carvacrol is mainly due to the activation of TRPV3. Hence, dyclonine ameliorates TRPV3 hyperactivity-caused scratching in a concentration-dependent manner. In conrast, dyclonine (10 μM) showed little effect on electrophysiological responses in mouse dorsal root ganglia (DRG) and trigeminal ganglia (TG) neurons (Figure 6—figure supplement 1). This observation is in line with the absence of TRPV3 in mouse DRGs (Peier et al., 2002), and suggest that the invio effect of dyclonine arises from the targeting of keratinocyte TRPV3 channels.

We also used wild-type and TRPV3 KO mice to examine the effect of dyclonine on thermal nociceptive responses to the noxious temperature 55 °C. In wild-type mice, dyclonine exhibited a tendency to reduce the nociceptive response (Figure 6—figure supplement 1). TRPV3 KO reduced mice nociceptive response to heating as compared to wild-type mice (55 °C; comparison between gray bars in Figure 6—figure supplement 1E). However, in TRPV3 KO mice, dyclonine showed no further effect, showing that dyclonine mainly targets TRPV3 in vivo. These observations also suggest that TRPV3 partially contributes to pain sensation in

thermal nociception, in consistency with the temperature-dependent responses of TRPV3 channel (Figure 4).

Effects of dyclonine on single TRPV3 channel activity

We then examined the functional and molecular mechanisms underlying the inhibition of TRPV3 by dyclonine. To distinguish whether such inhibition arises from the changes in channel gating or conductance, we measured single-channel activity. Single-channel recordings were performed in an inside-out patch that was derived from HEK 293T cells expressing the mouse TRPV3 (Figure 7). Currents were evoked by 10 μM 2-APB in the absence and presence of dyclonine (30 μM) after sensitization induced by 300 μM 2-APB at a holding potential of either +60 mV or -60 mV (Figure 7A). To quantify the changes, we constructed all-point histograms and measured the open probabilities and the unitary current amplitudes by Gaussian fitting. We observed that the single-channel open probability was largely decreased by dyclonine from 0.8 ± 0.02 to 0.08 ± 0.01 at -60 mV and from 0.82 ± 0.02 to 0.12 ± 0.01 at +60 mV (n = 6), respectively (Figure 7B). Statistical analysis, however, revealed that dyclonine had no effect on single TRPV3 channel conductance (163.6 ± 6.4 pS v.s. 179.2 ± 5.5 pS for before and after dyclonine treatment; Figure 7C).

The mechanism underlying the inhibition of TRPV3 by dyclonine

In order to understand the molecular mechanism underlying the blockade of TRPV3 by dyclonine, we utilized in *silico* docking to predict their interactions. The inhibitory effect of drugs on ion channels is usually achieved in three ways, competitively binding with agonists, negative allosteric regulation or directly blocking the channel pore. Dyclonine inhibited TRPV3 currents evoked by both 2-APB (Figure 1) and heat (Figure 4), implying that dyclonine is not a competitive antagonist. In addition, the voltage independence of dycloine inhibition and the fact that dyclonine is a positive charged alkaloid suggests that dyclonine is not simply an open channel blocker. Previous studies have demonstrated that local anesthetics inhibit voltage-gated sodium channels through a common drug-binding region within the channel pore (Tikhonov & Zhorov, 2017). We therefore suspected that the inhibition effect of dyclonine is also due to its allosteric interaction with specific residues within the aqueous pore of TRPV3. The grid file of in *silico* docking was then constructed to examine residues in the upper pore region and the central cavity of TRPV3 (Figure 8—figure supplement 1A); the best receptor–ligand complex was evaluated using the extra precision (XP) scoring. Ligand clusters derived from XP docking suggested three potential TRPV3/dyclonine binding modes (BMs): BM_A, BM_B and BM_C (Figure 8A-B). Moreover, residues within 10 Å of dyclonine poses were extensively refined using Induce-Fit-Docking (IFD) based on mTRPV3 cryo-EM structure (Singh, McGoldrick, & Sobolevsky, 2018) (Figure 8A - Figure 8—figure supplement 1B). BM_B and BM_C modes predicted that dyclonine occupies the ion permeation pathway behaving as an open channel blocker. This, however, contradicts with the fact that

dyclonine is a positive charged alkaloid (Figure 8B) and its inhibition effect is voltage-independent (Figure 3). Hence, BM_B and BM_C binding modes appear unlikely. Nevertheless, mutants in key residues in these two binding sites diversely affected the inhibition of dyclonine (I637A, IC_{50} = 6.1 ± 0.43 μM; F666A, IC_{50} = 414.5 ± 15.7 μM; I674A, IC_{50} = 15.1 ± 2.1 μM, Figure 8—figure supplement 1E-H), suggesting the pore region is crucial for dyclonine inhibition.

BM_A mode shows that dyclonine makes contacts with the cavity formed by the pore loop and S6-helix of TRPV3 (Figure 8A-B). Structures assigned to *apo* and open states revealed remarkable allosteric changes and cavity size reduction in these regions (Figure 8—figure supplement 1G-H), supporting the rationality of the BM_A mode.

To further delineate dyclonine-interacting residues, we systematically mutated the residues in the cavity of TRPV3 channel predicted by BM_A binding mode. Among the mutants, mutations L630W, N643A, I644W and L655A greatly reduced the inhibitory effect of dyclonine, whereas the mutants L642A and I659A showed higher sensitivity to dyclonine than wild-type channel (Figure 8C-D). The dose-response curves were fitted with a Hill equation, and the corresponding IC_{50} values for each TRPV3 mutant were as follows: IC_{50} = 286.7 ± 10.4 μM for L655A; IC_{50} = 30.8 ± 2.2 μM for L630W; IC_{50} = 37.7 ± 5.1 μM for N643A; IC_{50} = 26.1 ± 2.8 μM for I644W; IC_{50} = 0.25 ± 0.02 μM for L642A and IC_{50} = 0.56 ± 0.06 μM for I659A, compared to IC_{50} = 3.2 ± 0.24 μM for WT TRPV3 (Figure 8D-E). Notably, all mutant channels except L639A were functional and produced robust responses to 2-APB (Figure 8F). Covalent

modification of L630C, F633C and L642C, with side chains toward the proposed binding site, using MTSET (2-(trimethylammonium) ethyl methanethiosulfonate, bromide), an MTS reagent with bulk positive side chain, significantly decreased 2-APB-idnuced current in the mutated mTRPV3 channels (Figure 8G-H). The reduction reagent dithiothreitol (DTT) rescued this inhibitory effect, indicating that the interruption of the allostery of the pore cavity has impaired the channel activation of mTRPV3 (Figure 8G-H). In contrast, MTSET treatment had no effect on the activation of wild-type TRPV3 (Figure 8H). Along the same line, MTSET modification caused reduced dyclonine blockade in L630C, F633C and L642C but not wild-type TRPV3, and DTT restored the blockage of dyclonine in these mutants (Figure 8I), implying dyclonine-mediated inhibition is mediated by the region predicted by BM_A binding mode. Together, our results suggest that dyclonine interacts with the pore cavity of TRPV3 to prevent, likely behaving as a negative allosteric modulator.

Discussion

As a multimodal sensory channel, TRPV3 is abundantly expressed in keratinocytes and implicated in inflammatory skin disorders, itch, hair morphogenesis, and pain sensation (Broad et al., 2016). Human Olmsted syndrome has been linked to the gain-of-function mutations of TRPV3 (Agarwala et al., 2016; Lai-Cheong et al., 2012; Lin et al., 2012). Synthetic and natural compounds, like isopentenyl pyrophosphate (Bang, Yoo, Yang, Cho, & Hwang, 2011), 17(R)-resolvin D1 (Bang, Yoo, Yang, Cho, & Hwang, 2012), forsythoside B (Zhang et al., 2019), diphenyltetrahydrofuran osthole (Higashikawa et al., 2015) and ruthenium red (Xu et al., 2002) have been proposed to inhibit TRPV3 channels. Due to either or both the lack of targeting specificity and the clinical application, their remedial potential remains to be determined. Hence, identifying and understanding clinical pharmaceutics that target TRPV3 channels will help to conceive therapeutic interventions.

Dyclonine is a topical antipruritic agent and has been used for clinical treatment of itching and pain for decades (Gargiulo, Burns, & Huck, 1992; Greifenstein, Harris, & Parry, 1956). While the therapeutic effect of dyclonine has been attributed to the inhibition of cell depolarization, the underlying mechanisms have not been fully understood. In the present study, we provide several tiers of evidence that dyclonine potently inhibits TRPV3 channel. Such inhibition was observed for TRPV3 responses to both chemical and thermal activation, suggesting dyclonine is a condition-across inhibitor. Accordingly, dyclonine efficiently blocked the excessive activation of TRPV3 mutants and prevented cell death. Single-channel recordings revealed that

dyclonine effectively suppresses the channel open probability without changing single-channel conductance. These data not only supplement a molecular mechanism for the therapeutic effect of dyclonine, but also suggest its application to curb TRPV3-related disorders. Using mouse model, we indeed observed that dyclonin ameliorates the TRPV3 hyperactivity-caused itch/scratching behaviors, indicating its therapeutic inhibition effect being maintained in *vivo*. As TRPV3 responds to moderate temperatures (30 - 40 °C), dyclonine may thus be used to alleviate skin inflammations persisted in physiological temperatures. Also, as a clinical drug dyclonine has been widely used and thus has shown its safety to human body (Gargiulo et al., 1992; Sahdeo et al., 2014). In addition, as a potent inhibitor, dyclonine can also be a research tool to dissect the physio- and pathological characteristics of TRPV3 channel. While dyclonie effectively inhibits TRPV3 channels, our current results do not exclude its targeting of other molecular pathways. For instance, voltage-gated sodium channels have been shown to be inhibited by local anesthetics including dyclonine (Sahdeo et al., 2014; Tikhonov & Zhorov, 2017).

The current data also provide clues on the molecular mechanism underlying the inhibition of TRPV3 by dyclonine. The residues within the pore loop and S6-helix of TRPV3, as suggested by BM_A binding mode, create a functional 'hotspot' contributing to the inhibition of dyclonine. Chemical modification experiment further confirmed the importance of this 'hotspot' to channel gating and dyclonine inhibition. Interestingly, the size of pocket BM_A is distinct in the apo/resting and open states. Likely, binding of dyclonine into this pocket could prevent the structural

rearrangements of pore loop during TRPV3 gating, implying that dyclonine behaves as a negative allosteric modulator. Although similar pockets can also be observed on other TRP channels, the amino acids that make up the pocket and the precise shape of the pocket are diverse (Figure 8—figure supplement 2). This may be the reason why TRPV3 is targeted by dyclonine (Liao, Cao, Julius, & Cheng, 2013; Shimada et al., 2020; Singh et al., 2018). F666 is located below the upper filter and behaves with a bulky hydrophobic side chain, which may play a role in maintaining the shape of BM_A at the open state. This may be the reason why F666A is capable of decreasing the inhibition of dyclonine. Our current study revealed critical residues located within the pore cavity of TRPV3 that regulate dyclonine inhibition, yet the possibility exists that dyclonine inhibition is mediated by indirect mechanisms involving interactions with other residues. Nevertheless, the molecular sites uncovered by the present study would be instrumental for pinpointing the dyclonine-TRPV3 interaction at the molecular level, thereby developing specific therapeutics for chronic pruritus, dermatitis and skin inflammations.

Material and Methods

Key resources table

Reagent type (species) or resource	Designation	Source or reference	Identifiers	Additional information
Species (*Mus musculus*)	*Trpv3*$^{-/-}$ mice	(Wang et al., 2020)	PMID: 32535744	C57BL/6J background
Cell line (*Homo sapiens*)	HEK 293T	ATCC	Cat.#:CRL-3216	
Cell line (*Homo sapiens*)	T-Rex 293	Thermo Fisher	Cat.#:R71007	
Chemical compound	2-APB	Sigma-Aldrich	Cat.#:D9754	TRPV1-3 agonist
Chemical compound	Carvacrol	MedChemExpress	Cat.#:499752	TRPV3 agonist
Chemical compound	Menthol	Sigma-Aldrich	Cat.#:M278	TRPM8 agonist
Chemical compound	Capsaicin	MedChemExpress	Cat.#: HY10448	TRPV1 agonist
Chemical compound	AITC	Sigma-Aldrich	Cat.#:377430	TRPA1 agonist
Chemical compound	Ruthenium Red	Sigma-Aldrich	Cat.#:R2751	TRP channels inhibitor
Chemical compound	Poly-L-lysine hydrochloride	Sigma-Aldrich	Cat.#:2658	

Chemical compound	MTEST	MedChemExpress	Cat.#: 690632554
Chemical compound	DTT	Sigma-Aldrich	Cat.#: 3483123
Chemical compound	Dyclonine	MedChemExpress	Cat.#: 536436
Software, algorithm	Patchmaster	HEKA Electronics	
Software, algorithm	OriginPro	Originlab.com	
Software, algorithm	Clampfit 10	Molecular Devices	
Software, algorithm	SigmaPlot 10	SPSS Science	

cDNA constructs and transfection in HEK 293T cells

The wild-type mouse TRPV3 (mTRPV3), human TRPV3 (hTRPV3), rat TRPV1, rat TRPV2, rat TRPM8 and mouse TRPA1 cDNAs were generously provided by Dr. Feng Qin (State University of New York at Buffalo, Buffalo, USA). The GFP-mTRPV3 wild-type and the mutants (mTRPV3-G573S and mTRPV3-G573C) in pcDNA4/TO vector were gifts from Dr. Michael X. Zhu (The University of Texas Health Science Center at Houston, Houston, USA). The wild-type frog TRPV3 (fTRPV3) was kindly provided by Dr. Makoto Tominaga (Department of Physiological Sciences, SOKENDAI, Okazaki, Japan). All mutations were made using the overlap-extension polymerase chain reaction (PCR) method as previously

455 described (Tian et al., 2019). The resulting mutations were then verified by DNA
456 sequencing. HEK 293T and T-Rex 293 cells were grown in Dulbecco's modified
457 Eagles medium (DMEM, Thermo Fisher scientific, MA, USA) containing 4.5 mg/ml
458 glucose, 10% heat-inactivated fetal bovine serum (FBS), 50 units/ml penicillin, and
459 50 mg/ml streptomycin, and were incubated at 37^{o}C in a humidified incubator gassed
460 with 5% CO_2. For T-Rex 293, blasticidin S (10 μg/ml) was also included. Cells grown
461 into ~80% confluence were transfected with the desired DNA constructs using either
462 the standard calcium phosphate precipitation method or lipofectamine 2000
463 (Invitrogen) following the protocol provided by the manufacturer. Transfected HEK
464 293T cells were reseeded on 12 mm round glass coverslips coated by poly-L-lysine.
465 Experiments took place ~12-24 h after transfection.

466 **Cell lines**

467 HEK 293T and T-Rex 293 cell lines used in this study were respectively from the
468 American Type Culture Collection and Thermo Fisher, authenticated by STR locus
469 and tested negative for mycoplasma contamination.

470

471 **Mouse epidermal keratinocyte culture**

472 The animal protocol used in this study was approved by the Institutional Animal Care
473 and Use Committee of Wuhan University. Primary mouse keratinocytes were
474 prepared according to the method previously described (Luo, Stewart, Berdeaux, &
475 Hu, 2012; Pirrone, Hager, & Fleckman, 2005). Briefly, newborn wild-type C57B/6
476 mice (postnatal day 1–3) were deeply anaesthetized and decapitated and then soaked

in 10% povidone-iodine, 70% ethanol, and phosphate-buffered saline for 5 min, respectively. The skin on the back was removed and rinsed with pre-cold sterile phosphate-buffered saline (PBS) in a 100-mm Petri dish and transferred into a 2-ml tube filled with pre-cold digestion buffer containing 4 mg/ml dispase II and incubated overnight at 4 °C. After treatment with dispase II for 12-18 h, the epidermis was gently peeled off from dermis and collected. Keratinocytes were dispersed by gentle scraping and flushing with KC growth medium (Invitrogen, Carlsbad, CA). The resulting suspension of single cells was collected by centrifuge and, cells were seeded onto coverslips pre-coated with poly-L-lysine, and maintained in complete keratinocyte serum-free growth medium (Invitrogen, Carlsbad, CA). Cell culture medium was refreshed every two days. Patch-clamp recordings were carried out 48 h after plating.

Electrophysiological recording

Conventional whole-cell and excised patch-clamp recording methods were used. For the recombinant expressing system, green fluorescent EGFP was used as a surface marker for gene expression. Recording pipettes were pulled from borosilicate glass capillaries (World Precision Instruments), and fire-polished to a resistance between 2–4 MΩ when filled with internal solution containing (in mM): 140 CsCl, 2.0 $MgCl_2$, 5 EGTA, 10 HEPES, pH 7.4 (adjusted with CsOH). Bath solution contained (in mM): 140 NaCl, 5 KCl, 3 EGTA, and 10 HEPES, pH 7.4 adjusted with NaOH. For recordings in keratinocytes, the bath saline consisted of (in mM) 140 NaCl, 5 KCl, 2 $MgCl_2$, 2 $CaCl_2$, 10 glucoses, 10 HEPES, pH 7.4 adjusted with NaOH and the pipette

499 solution contained (in mM): 140 CsCl, 5 EGTA, and 10 HEPES, pH 7.3 adjusted with
500 CsOH. For single-channel recordings, the pipette solution and bath solution were
501 symmetrical and contained (in mM) 140 NaCl, 5 KCl, 3 EGTA, 10 HEPES, pH 7.4.
502 Isolated cells were voltage clamped and held at -60 mV using an EPC10 amplifier
503 with the Patchmaster software (HEKA, Lambrecht, Germany). For a subset of
504 recordings, currents were amplified using an Axopatch 200B amplifier (Molecular
505 Devices, Sunnyvale, CA) and recorded through a BNC-2090/MIO acquisition system
506 (National Instruments, Austin, TX) using QStudio developed by Dr. Feng Qin at State
507 University of New York at Buffalo. Whole-cell recordings were typically sampled at 5
508 kHz and filtered at 1 kHz, and single-channel recordings were sampled at 25 kHz and
509 filtered at 10 kHz. The compensation of pipette series resistance and capacitance were
510 compensated using the built-in circuitry of the amplifier (>80%) to reduce voltage
511 errors. Exchange of external solution was performed using a gravity-driven local
512 perfusion system. As determined by the conductance tests, the solution around a patch
513 under study was fully controlled by the application of a flow rate of 100 μl/min or
514 greater. Dyclonine hydrochloride, MTSET (2-(trimethylammonium)ethyl
515 methanethiosulfonate, bromide) and carvacrol were purchased from MCE (Med Chem
516 Express). Unless otherwise noted, all chemicals were purchased from Sigma
517 (Millipore Sigma, St. Louis, MO). Water-insoluble reagents were dissolved in pure
518 ethanol or DMSO to make a stock solution and diluted into the recording solution at
519 the desired final concentrations before the experiment. The final concentrations of
520 ethanol or DMSO did not exceed 0.3%, which had no effect to currents. In the

scratching behavior experiments, carvacrol was firstly dissolved in 10% ethanol and then diluted in normal saline before administration. All experiments except those for heat activation were performed at room temperature (22-24℃).

Ultrafast temperature jump achievement

Rapid temperature jumps were generated by the laser irradiation approach as described previously(Yao, Liu, & Qin, 2009). In brief, a single emitter infrared laser diode (1470 nm) was used as a heat source. A multimode fiber with a core diameter of 100 μm was used to transmit the launched laser beam. The other end of the fiber exposed the fiber core was placed close to cells as the perfusion pipette is typically positioned. The laser diode driven by a pulsed quasi-CW current powder supply (Stone Laser, Beijing, China). Pulsing of the controller was controlled from computer through the data acquisition card using QStudio software developed by Dr. Feng Qin at State University of New York at Buffalo. A blue laser line (460 nm) was coupled into the fiber to aid alignment. The beam spot on the coverslip was identified by illumination of GFP-expressing cells using the blue laser during experiment.

Constant temperature steps were generated by irradiating the tip of an open pipette and using the current of the electrode as the readout for feedback control. The laser was first powered on for a brief duration to reach the target temperature and was then modulated to maintain a constant pipette current. The sequence of the modulation pulses was stored and subsequently played back to apply temperature jumps to the cell of interest. Temperature was calibrated offline from the pipette current using the

dependence of electrolyte conductivity.

Cell death analysis by flow cytometry

T-Rex 293 cells were grown in DMEM containing 4.5 mg/ml glucose, 10% (vol/vol) FBS, 50 units/ml penicillin, 50 μg/ml streptomycin, and blasticidin S (10 μg/ml) and were incubated at 37°C in a humidified incubator gassed with 5% CO_2. Transfections were performed in wells of a 24-well plate using lipofectamine 2000 (Invitrogen). The GFP-TRPV3 (wild-type and G573 mutants) cDNAs in pcDNA4/TO vector were individually transfected into T-Rex 293 cells and treated with 20 ng/ml doxycycline 16 h post-transfection to induce the gene expression following the method as previously described (Xiao et al., 2008). Expression of GFP fluorescence detected by an epifluorescence microscope was used as an indicator of gene expression. After treatments with the compounds for 12 h, cells were collected, washed twice with phosphate-buffered saline (PBS), resuspended and then dyed with propidium iodide (PI, Thermo Fisher Scientific) in the dark according to the manufacturer's instructions. The membrane integrity of the cells was assessed using a BD FACSCelesta flow cytometer equipped with BD Accuri C6 software (BD Biosciences, USA).

Evaluation of scratching behavior in mice

Behavioral studies were performed with six to eight-week-old wild-type or *Trpv3*$^{-/-}$ adult C57B/6 mice. To assess itch-scratching behaviors, the hair of the rostral part of the mouse right neck was shaved using an electric hair clipper 24 hours before the start of experiments. *Trpv3*$^{-/-}$ mice have been described previously (Wang et al., 2020).

563 Scratching behaviors were recorded on video. The number of itch-scratching bouts
564 was counted through video playback analysis. One scratching bout was defined as an
565 episode in which a mouse lifted its right hind limb to the injection site and scratched
566 continuously for any time length until this limb was returned to the floor or mouth
567 (Wilson et al., 2013). All behavioral experiments were conducted in a double-blind
568 manner. To examine acute scratching/itch induced by carvacrol or pruritogen
569 histamine, mice were firstly placed in an observation box (length, width, and height: 9
570 × 9 × 13 cm^3) for acclimatization for about 30 minutes. Then carvacrol (0.1%) in a
571 volume of 50 μl was injected intradermally into the right side of the mouse neck. To
572 access the effect of dyclonine on itch scratching, normal saline (0.9% NaCl) or
573 dyclonine (1, 10, and 50 μM) was injected intradermally 30 minutes before
574 intradermal injection of carvacrol (Cui et al., 2018; Sun & Dong, 2016). Behaviors
575 were recorded on video for 30 minutes following the injection of carvacrol.

576 **Hargreaves test for behavioral experiments**

577 All tests were conducted during the light phase of the light/dark cycle by a trained
578 observer blind to the genotype. Mice were habituated to the testing room for 60 min
579 prior to the behavioral tests unless otherwise stated. The Hargreaves test was
580 performed as described previously (Wang et al., 2018). All behavioral experiments
581 were conducted in a double-blind manner. For measure of thermal hyperalgesia,
582 animals were placed individually, 30 min after injection, on a hot plate (Bioseb,
583 Chaville, France) with the temperature adjusted to 55 ºC. The withdrawal latency of

each hind paw was determined until nocifensive reaction appeared (licking foot). Right hind paws of mice were injected intraplantarly with 10 μl normal saline (0.9% NaCl). Left hind paws of mice were injected intraplantarly with 10 μl normal saline (supplemented with 10 or 50 μM dyclonine).

Molecular docking

The molecular docking approach was used to model the interaction between dyclonine and TRPV3 channel protein (PDB ID code: 6DVZ) according to previous description (L. D. Huang et al., 2014; Li et al., 2018). The 3D structure of dyclonine was generated by LigPrep (Gadakar, Phukan, Dattatreya, & Balaji, 2007). Glide (Friesner et al., 2004) and Induce-Fit-Docking (IFD) (Sherman, Day, Jacobson, Friesner, & Farid, 2006) was employed to dock dyclonine into the potential binding. For Glide docking, the grid for the protein was defined as an enclosing cubic box within 34 Å to include upper pore region and the central cavity of TRPV3, and the extra precision (XP) docking mode was selected. During in silico docking, at most 100000 poses passed through for the initial phase of docking, among of which top 300 poses were processed with post-docking minimization. The threshold for rejecting minimized pose was set to 0.5 kcal/mol. A maximum of 200 poses were finally written out. The docking scores and dyclonine-residue interaction distance were summarized, sorted and then plotted by Maestro. Induced fit docking was performed to refine the interaction between dyclonine and TRPV3 (Sherman et al., 2006), L655, I674 and G638 residues were chosen from the center of the docking box, respectively. During this docking process, the protein and the dyclonine were both flexible. All

structural figures were made by PyMol (http://www.pymol.org).

Statistics

Data were analyzed offline with Clampfit (Molecular Devices, Sunnyvale, CA), IGOR (Wavemetrics, Lake Oswego, OR, USA), SigmaPlot (SPSS Science, Chicago, IL, USA) and OriginPro (OriginLab Corporation, MA, USA). For concentration dependence analysis, the modified Hill equation was used: $Y = A1 + (A2 - A1) / (1 + (IC_{50} / [toxin])^{nH})$, in which IC_{50} is the half maximal effective concentration, and n_H is the Hill coefficient. Unless stated otherwise, the data are expressed as mean ± standard error (SEM), from a population of cells (*n*), with statistical significance assessed by Student's *t*-test for two-group comparison or one-way analysis of variance (ANOVA) tests for multiple group comparisons. Significant difference is indicated by a *p* value less than 0.05 (*$p < 0.05$, **$p < 0.01$).

Acknowledgements

We are grateful to our colleagues and members of Yao lab for comments and discussions, and we also would like to thank the core facilities of College of Life Sciences at Wuhan University for technical help. This work was supported by grants from the National Natural Science Foundation of China (31830031, 31929003, 31871174, 31671209 and 31601864), Natural Science Foundation of Hubei Province (2017CFA063 and 2018CFA016), the Fundamental Research Funds for the Central Universities, the Natural Science Foundation of Jiangsu Province (BK20202002), Innovation and Entrepreneurship Talent Program of Jiangsu Province, and State Key Laboratory of Utilization of Woody Oil Resource with grant number 2019XK2002.

Conflict of Interest

The authors declare that they have no conflict of interest.

References

Agarwala, M. K., George, R., Pramanik, R., & McGrath, J. A. (2016). Olmsted syndrome in an Indian male with a new de novo mutation in TRPV3. *Br J Dermatol, 174*(1), 209-211. doi:10.1111/bjd.13910

Aijima, R., Wang, B., Takao, T., Mihara, H., Kashio, M., Ohsaki, Y., . . . Kido, M. A. (2015). The thermosensitive TRPV3 channel contributes to rapid wound healing in oral epithelia. *Faseb j, 29*(1), 182-192. doi:10.1096/fj.14-251314

Asakawa, M., Yoshioka, T., Matsutani, T., Hikita, I., Suzuki, M., Oshima, I., . . . Sakata, T. (2006). Association of a mutation in TRPV3 with defective hair growth in rodents. *J Invest Dermatol, 126*(12), 2664-2672. doi:10.1038/sj.jid.5700468

Bang, S., Yoo, S., Yang, T. J., Cho, H., & Hwang, S. W. (2011). Isopentenyl pyrophosphate is a novel antinociceptive substance that inhibits TRPV3 and TRPA1 ion channels. *Pain, 152*(5), 1156-1164. doi:10.1016/j.pain.2011.01.044

Bang, S., Yoo, S., Yang, T. J., Cho, H., & Hwang, S. W. (2012). 17(R)-resolvin D1 specifically inhibits transient receptor potential ion channel vanilloid 3 leading to peripheral antinociception. *Br J Pharmacol, 165*(3), 683-692. doi:10.1111/j.1476-5381.2011.01568.x

Borbiro, I., Lisztes, E., Toth, B. I., Czifra, G., Olah, A., Szollosi, A. G., . . . Biro, T. (2011). Activation of transient receptor potential vanilloid-3 inhibits human hair growth. *J Invest Dermatol, 131*(8), 1605-1614. doi:10.1038/jid.2011.122

Broad, L. M., Mogg, A. J., Eberle, E., Tolley, M., Li, D. L., & Knopp, K. L. (2016).

TRPV3 in Drug Development. *Pharmaceuticals (Basel), 9*(3). doi:10.3390/ph9030055

Cheng, X., Jin, J., Hu, L., Shen, D., Dong, X. P., Samie, M. A., . . . Xu, H. (2010). TRP channel regulates EGFR signaling in hair morphogenesis and skin barrier formation. *Cell, 141*(2), 331-343. doi:10.1016/j.cell.2010.03.013

Chung, M. K., Guler, A. D., & Caterina, M. J. (2005). Biphasic currents evoked by chemical or thermal activation of the heat-gated ion channel, TRPV3. *J Biol Chem, 280*(16), 15928-15941. doi:10.1074/jbc.M500596200

Chung, M. K., Lee, H., Mizuno, A., Suzuki, M., & Caterina, M. J. (2004a). 2-aminoethoxydiphenyl borate activates and sensitizes the heat-gated ion channel TRPV3. *Journal of Neuroscience, 24*(22), 5177-5182. doi:10.1523/Jneurosci.0934-04.2004

Chung, M. K., Lee, H., Mizuno, A., Suzuki, M., & Caterina, M. J. (2004b). 2-aminoethoxydiphenyl borate activates and sensitizes the heat-gated ion channel TRPV3. *J Neurosci, 24*(22), 5177-5182. doi:10.1523/JNEUROSCI.0934-04.2004

Chung, M. K., Lee, H., Mizuno, A., Suzuki, M., & Caterina, M. J. (2004c). TRPV3 and TRPV4 mediate warmth-evoked currents in primary mouse keratinocytes. *J Biol Chem, 279*(20), 21569-21575. doi:10.1074/jbc.M401872200

Clapham, D. E. (2003). TRP channels as cellular sensors. *Nature, 426*(6966), 517-524. doi:10.1038/nature02196

Colton, C. K., & Zhu, M. X. (2007). 2-Aminoethoxydiphenyl borate as a common

activator of TRPV1, TRPV2, and TRPV3 channels. *Handb Exp Pharmacol*(179), 173-187. doi:10.1007/978-3-540-34891-7_10

Cui, T. T., Wang, G. X., Wei, N. N., & Wang, K. W. (2018). A pivotal role for the activation of TRPV3 channel in itch sensations induced by the natural skin sensitizer carvacrol. *Acta Pharmacologica Sinica, 39*(3), 331-335. doi:10.1038/aps.2017.152

Duchatelet, S., Pruvost, S., de Veer, S., Fraitag, S., Nitschke, P., Bole-Feysot, C., . . . Hovnanian, A. (2014). A new TRPV3 missense mutation in a patient with Olmsted syndrome and erythromelalgia. *JAMA Dermatol, 150*(3), 303-306. doi:10.1001/jamadermatol.2013.8709

Florestano, H. J., & Bahler, M. E. (1956). Antimicrobial properties of dyclonine hydrochloride, a new topical anesthetic. *J Am Pharm Assoc Am Pharm Assoc, 45*(5), 320-325. doi:10.1002/jps.3030450514

Formaker, B. K., Mott, A. E., & Frank, M. E. (1998). The effects of topical anesthesia on oral burning in burning mouth syndrome. *Ann N Y Acad Sci, 855*, 776-780. doi:10.1111/j.1749-6632.1998.tb10657.x

Friesner, R. A., Banks, J. L., Murphy, R. B., Halgren, T. A., Klicic, J. J., Mainz, D. T., . . . Shenkin, P. S. (2004). Glide: A new approach for rapid, accurate docking and scoring. 1. Method and assessment of docking accuracy. *Journal of Medicinal Chemistry, 47*(7), 1739-1749. Retrieved from <Go to ISI>://WOS:000220317600019

Gadakar, P. K., Phukan, S., Dattatreya, P., & Balaji, V. N. (2007). Pose prediction

accuracy in docking studies and enrichment of actives in the active site of GSK-3beta. *J Chem Inf Model*, *47*(4), 1446-1459. doi:10.1021/ci6005036

Gao, L., Yang, P., Qin, P., Lu, Y., Li, X., Tian, Q., . . . Yao, J. (2016). Selective potentiation of 2-APB-induced activation of TRPV1-3 channels by acid. *Sci Rep*, *6*, 20791. doi:10.1038/srep20791

Gargiulo, A. V., Burns, G. M., & Huck, C. P. (1992). Dyclonine hydrochloride--a topical agent for managing pain. *Ill Dent J*, *61*(4), 303-304. Retrieved from http://www.ncbi.nlm.nih.gov/pubmed/1286862

Greifenstein, F. E., Harris, L. C., Jr., & Parry, J. C. (1956). Dyclonine; a new local anesthetic agent: clinical evaluation. *Anesthesiology*, *17*(5), 648-652. doi:10.1097/00000542-195609000-00002

Higashikawa, A., Kojima, Y., Sato, M., Kimura, M., Ogura, K., Mochizuki, H., . . . Tazaki, M. (2015). Transient Receptor Potential Cation Channel Subfamily Vanilloid Member 3 is not Involved in Plasma Membrane Stretch-induced Intracellular Calcium Signaling in Merkel Cells. *Bull Tokyo Dent Coll*, *56*(4), 259-262. doi:10.2209/tdcpublication.56.259

Ho, J. C., & Lee, C. H. (2015). TRP channels in skin: from physiological implications to clinical significances. *Biophysics (Nagoya-shi)*, *11*, 17-24. doi:10.2142/biophysics.11.17

Huang, L. D., Fan, Y. Z., Tian, Y., Yang, Y., Liu, Y., Wang, J., . . . Yu, Y. (2014). Inherent dynamics of head domain correlates with ATP-recognition of P2X4 receptors: insights gained from molecular simulations. *PLoS One*, *9*(5),

e97528. doi:10.1371/journal.pone.0097528

Huang, S. M., Lee, H., Chung, M. K., Park, U., Yu, Y. Y., Bradshaw, H. B., . . . Caterina, M. J. (2008). Overexpressed transient receptor potential vanilloid 3 ion channels in skin keratinocytes modulate pain sensitivity via prostaglandin E2. *J Neurosci, 28*(51), 13727-13737. doi:10.1523/JNEUROSCI.5741-07.2008

Lai-Cheong, J. E., Sethuraman, G., Ramam, M., Stone, K., Simpson, M. A., & McGrath, J. A. (2012). Recurrent heterozygous missense mutation, p.Gly573Ser, in the TRPV3 gene in an Indian boy with sporadic Olmsted syndrome. *Br J Dermatol, 167*(2), 440-442. doi:10.1111/j.1365-2133.2012.11115.x

Li, B., Wang, J., Cheng, X. Y., Liu, Y., Yang, Y., Yang, X. N., . . . Yu, Y. (2018). Molecular mechanism underlying the subtype-selectivity of competitive inhibitor NF110 and its distinct potencies in human and rat P2X3 receptors. *Science Bulletin, 63*(24), 1616-1625. Retrieved from <Go to ISI>://WOS:000455135400008

Liao, M., Cao, E., Julius, D., & Cheng, Y. (2013). Structure of the TRPV1 ion channel determined by electron cryo-microscopy. *Nature, 504*(7478), 107-112. doi:10.1038/nature12822

Lin, Z., Chen, Q., Lee, M., Cao, X., Zhang, J., Ma, D., . . . Yang, Y. (2012). Exome sequencing reveals mutations in TRPV3 as a cause of Olmsted syndrome. *Am J Hum Genet, 90*(3), 558-564. doi:10.1016/j.ajhg.2012.02.006

744 Luo, J., & Hu, H. (2014). Thermally activated TRPV3 channels. *Curr Top Membr, 74*,
745 325-364. doi:10.1016/b978-0-12-800181-3.00012-9
746 Luo, J., Stewart, R., Berdeaux, R., & Hu, H. (2012). Tonic inhibition of TRPV3 by
747 Mg2+ in mouse epidermal keratinocytes. *J Invest Dermatol, 132*(9),
748 2158-2165. doi:10.1038/jid.2012.144
749 Moqrich, A., Hwang, S. W., Earley, T. J., Petrus, M. J., Murray, A. N., Spencer, K.
750 S., . . . Patapoutian, A. (2005). Impaired thermosensation in mice lacking
751 TRPV3, a heat and camphor sensor in the skin. *Science, 307*(5714),
752 1468-1472. doi:10.1126/science.1108609
753 Morginson, W. J., Rich, C. O., Eskelson, Y. D., Kirkman, L. W., Utterback, M.,
754 Burton, A. M., & Coletti, J. M. (1956). Dyclonine hydrochloride: a new
755 topical antipruritic agent. *Postgrad Med, 19*(6), 605-607.
756 doi:10.1080/00325481.1956.11708352
757 Peier, A. M., Reeve, A. J., Andersson, D. A., Moqrich, A., Earley, T. J., Hergarden, A.
758 C., . . . Patapoutian, A. (2002). A heat-sensitive TRP channel expressed in
759 keratinocytes. *Science, 296*(5575), 2046-2049. doi:10.1126/science.1073140
760 Pirrone, A., Hager, B., & Fleckman, P. (2005). Primary mouse keratinocyte culture.
761 *Methods Mol Biol, 289*, 3-14. doi:10.1385/1-59259-830-7:003
762 Sahdeo, S., Scott, B. D., McMackin, M. Z., Jasoliya, M., Brown, B., Wulff, H., . . .
763 Cortopassi, G. A. (2014). Dyclonine rescues frataxin deficiency in animal
764 models and buccal cells of patients with Friedreich's ataxia. *Hum Mol Genet,*
765 *23*(25), 6848-6862. doi:10.1093/hmg/ddu408

766 Sherman, W., Day, T., Jacobson, M. P., Friesner, R. A., & Farid, R. (2006). Novel
767 procedure for modeling ligand/receptor induced fit effects. *J Med Chem, 49*(2),
768 534-553. doi:10.1021/jm050540c
769 Shimada, H., Kusakizako, T., Dung Nguyen, T. H., Nishizawa, T., Hino, T., Tominaga,
770 M., & Nureki, O. (2020). The structure of lipid nanodisc-reconstituted TRPV3
771 reveals the gating mechanism. *Nat Struct Mol Biol, 27*(7), 645-652.
772 doi:10.1038/s41594-020-0439-z
773 Singh, A. K., McGoldrick, L. L., & Sobolevsky, A. I. (2018). Structure and gating
774 mechanism of the transient receptor potential channel TRPV3. *Nat Struct Mol*
775 *Biol, 25*(9), 805-813. doi:10.1038/s41594-018-0108-7
776 Sun, S., & Dong, X. (2016). Trp channels and itch. *Semin Immunopathol, 38*(3),
777 293-307. doi:10.1007/s00281-015-0530-4
778 Tian, Q., Hu, J., Xie, C., Mei, K., Pham, C., Mo, X., . . . Yao, J. (2019). Recovery
779 from tachyphylaxis of TRPV1 coincides with recycling to the surface
780 membrane. *Proc Natl Acad Sci U S A, 116*(11), 5170-5175.
781 doi:10.1073/pnas.1819635116
782 Tikhonov, D. B., & Zhorov, B. S. (2017). Mechanism of sodium channel block by
783 local anesthetics, antiarrhythmics, and anticonvulsants. *J Gen Physiol, 149*(4),
784 465-481. doi:10.1085/jgp.201611668
785 Wang, Y., Gao, Y., Tian, Q., Deng, Q., Wang, Y., Zhou, T., . . . Li, Y. (2018). TRPV1
786 SUMOylation regulates nociceptive signaling in models of inflammatory pain.
787 *Nat Commun, 9*(1), 1529. doi:10.1038/s41467-018-03974-7

Wang, Y., Li, H., Xue, C., Chen, H., Xue, Y., Zhao, F., . . . Cao, Z. (2020). TRPV3 enhances skin keratinocyte proliferation through EGFR-dependent signaling pathways. *Cell Biol Toxicol*. doi:10.1007/s10565-020-09536-2

Wilson, S. R., The, L., Batia, L. M., Beattie, K., Katibah, G. E., McClain, S. P., . . . Bautista, D. M. (2013). The epithelial cell-derived atopic dermatitis cytokine TSLP activates neurons to induce itch. *Cell, 155*(2), 285-295. doi:10.1016/j.cell.2013.08.057

Xiao, R., Tian, J., Tang, J., & Zhu, M. X. (2008). The TRPV3 mutation associated with the hairless phenotype in rodents is constitutively active. *Cell Calcium, 43*(4), 334-343. doi:10.1016/j.ceca.2007.06.004

Xu, H., Delling, M., Jun, J. C., & Clapham, D. E. (2006). Oregano, thyme and clove-derived flavors and skin sensitizers activate specific TRP channels. *Nat Neurosci, 9*(5), 628-635. doi:10.1038/nn1692

Xu, H., Ramsey, I. S., Kotecha, S. A., Moran, M. M., Chong, J. A., Lawson, D., . . . Clapham, D. E. (2002). TRPV3 is a calcium-permeable temperature-sensitive cation channel. *Nature, 418*(6894), 181-186. doi:10.1038/nature00882

Yamada, T., Ueda, T., Ugawa, S., Ishida, Y., Imayasu, M., Koyama, S., & Shimada, S. (2010). Functional expression of transient receptor potential vanilloid 3 (TRPV3) in corneal epithelial cells: involvement in thermosensation and wound healing. *Exp Eye Res, 90*(1), 121-129. doi:10.1016/j.exer.2009.09.020

Yamamoto-Kasai, E., Imura, K., Yasui, K., Shichijou, M., Oshima, I., Hirasawa, T., . . . Yoshioka, T. (2012). TRPV3 as a therapeutic target for itch. *J Invest Dermatol,*

132(8), 2109-2112. doi:10.1038/jid.2012.97

Yao, J., Liu, B., & Qin, F. (2009). Rapid temperature jump by infrared diode laser irradiation for patch-clamp studies. *Biophys J, 96*(9), 3611-3619. doi:10.1016/j.bpj.2009.02.016

Zhang, H., Sun, X., Qi, H., Ma, Q., Zhou, Q., Wang, W., & Wang, K. (2019). Pharmacological Inhibition of the Temperature-Sensitive and Ca(2+)-Permeable Transient Receptor Potential Vanilloid TRPV3 Channel by Natural Forsythoside B Attenuates Pruritus and Cytotoxicity of Keratinocytes. *J Pharmacol Exp Ther, 368*(1), 21-31. doi:10.1124/jpet.118.254045

Figure legends

Figure 1. Inhibition of TRPV3 currents by dyclonine.

(**A**) Inhibition of 2-APB-evoked currents by dyclonine (Dyc) in a representative HEK 293T cell expressing mouse TRPV3. After sensitization by repeated application of 100 μM 2-APB, the cell was exposed to 5 or 10 μM dyclonine with 100 μM 2-APB or 10 μM dyclonine only as indicated by the bars. Membrane currents were recorded in whole-cell configuration, and the holding potential was -60 mV. (**B**) Summary of relative currents elicited by 100 μM 2-APB in the presence of 0, 5 or 10 μM dyclonine. Numbers of cells are indicated in parentheses. (**C**) The dose-response curve for dyclonine inhibition of TRPV3 currents was fitted by Hill's equation (IC_{50} = 3.2 ± 0.24 μM and n_H = 2.2 ± 0.32, *n* = 6). (**D**) Representative whole-cell current traces showing the responses to varying concentrations of 2-APB without or with 3 μM dyclonine after full sensitization of TRPV3. (**E**) Concentration-response curves of 2-APB without or with dyclonine. Data are shown as relative values to the current evoked by 300 μM 2-APB. Solid lines are fits to Hill equation, yielding EC_{50} = 22.93 ± 0.02 μM and n_H = 1.6 ± 0.1 without dyclonine (*n* = 6); and EC_{50} = 22.03 ± 0.86 μM and n_H = 1.7 ± 0.1 with 3 μM dyclonine (*n* = 6). (**F**) Dose-response curves normalized to its own maximum of each condition. (**G**-**H**) Representative whole-cell recordings for the sensitization of TRPV3 currents elicited by repeated applications of 100 μM 2-APB in the absence (**G**) and presence (**H**) of 5 μM dyclonine. (**I**) Time courses toward the peak currents elicited by repeated application of 100 μM 2-APB with or without dyclonine (*n* = 9). Currents were normalized to each initial values. (**J**) The

2-APB-evoked inward currents were reversibly inhibited by dyclonine in primary mouse epidermal keratinocytes. Representative inward currents were firstly activated by repeated application of 300 μM 2-APB at the holding potential of -60 mV, and then inhibited by 5 or 30 μM dyclonine or 10 μM Ruthenium Red (RR) as indicated. (**K**) Summary of relative currents elicited by 300 μM 2-APB with or without dyclonine. (**L**) Dose dependence of dyclonine effects on TRPV3 currents in cultured keratinocytes. The solid line corresponds to a fit by Hill's equation with IC_{50} = 5.2 ± 0.71 μM and n_H = 2.4 ± 0.75 (*n* = 6). The dotted line indicates zero current level.

Figure 2. Dyclonine is a potent inhibitor of TRPV3 channel.

(**A**) Representative inward current traces from whole-cell voltage-clamp recordings show the inhibitory effects of 10 μM dyclonine on TRPV1 (**A_1**), TRPV2 (**A_2**), TRPV3 (**A_3**), TRPM8 (**A_4**) or TRPA1 (**A_5**) channels (Dyc, dyclonine; Cap, capsaicin; Men, menthol). Bars represent duration of drug application. (**B**) Summary of relative currents before and after dyclonine (10 μM) treatment. Numbers of cells are indicated in parentheses. (**C**) Dose-response curves of dyclonine for inhibition of indicated ion channel currents. Solid lines represent fits by Hill equation, with IC_{50} = 337.4 ± 19.4 μM and n_H = 2.0 ± 0.31 for TPRV1 (*n* = 7), IC_{50} = 31.1 ± 2.7 μM and n_H = 2.9 ± 0.50 for TPRV2 (*n* = 8), IC_{50} = 81.8 ± 12.7 μM and n_H = 1.2 ± 0.20 for TRPM8 (*n* = 6), IC_{50} = 154.7 ± 15.6 μM and n_H = 1.3 ± 0.15 for TRPA1 (*n* = 6). For comparison, the dose-response curve of TRPV3 channel from Figure 1C is displayed in red with IC_{50} = 3.2 ± 0.24 μM and n_H = 2.2 ± 0.32 (*n* = 6). (**D**) Suppression of 2-APB-evoked

currents by dyclonine in a hTRPV3-expressing HEK293T cell. Representative inward current trace shows the reversible block effect of dyclonine (30 and 50 μM) at the holding potential of -60 mV. (**E**) Summary of inhibition of hTRPV3 by dyclonine. Membrane currents were normalized to the responses elicited by the saturated concentration of 2-APB (100 μM) alone. (**F**) Dose-response curve for dyclonine on blocking of hTRPV3. Solid line represents a fit to a Hill equation, yielded IC_{50} = 16.2 ± 0.72 μM and n_H = 1.91 ± 0.14 (*n* = 11). (**G**) Inhibition of fTRPV3 currents by dyclonine. Representative whole-cell currents at -60 mV in a fTRPV3-expressing HEK293T cell. After sensitization by repeated application of 3 mM 2-APB, the cell was exposed sequentially to 15 and 30 μM dyclonine with 3 mM 2-APB. (**H**) Summary of inhibition of relative currents elicited by 3 mM 2-APB, 3 mM 2-APB with dyclonine 15 or 30 μM. (**I**) Concentration-response curve of dyclonine on the inhibition of fTRPV3 currents. Solid line represents a fit by a Hill equation, with IC_{50} = 12.31 ± 1.6 μM and n_H = 1.6 ± 0.34 (*n* = 7). The dotted line indicates zero current level. Dyc, dyclonine; hTRPV3, human TRPV3; fTRPV3, frog TRPV 3.

Figure 3. The inhibitory effect of dyclonine on TRPV3 channel is voltage-independent.

(**A**) Representative whole-cell currents evoked by voltage steps (*inset*) together with 40 μM 2-APB in the absence and presence of 10, 30 μM dyclonine or 10 μM RR in HEK 293T cells expressing mouse TRPV3. Currents were elicited with 200-ms test

pulses ranging from -160 mV to +180 mV in 20-mV increments within the same cells, and the holding potential was -60 mV. Calcium-free standard bath solution and a CsCl-filled recording electrode were used. The dotted line indicates zero current level. (**B**) Current-voltage relations for data in (**A**). Current amplitudes were normalized to the maximum responses at +180 mV in the presence of 40 μM 2-APB. Each point represents mean values (± SEM) from eight independent cells. (*Inset*) The inhibition effects of dyclonine and RR on TRPV3 currents at negative holding potentials is magnified and displayed on the right. Note that dyclonine had an inhibitory effect on TRPV3 currents at both positive and negative potentials, but RR only inhibited TRPV3 channel currents at negative potentials while enhanced TRPV3 currents at positive potentials (blue trace). (**C**) Percentage block of TRPV3 currents by dyclonine (10 and 30 μM) as a function of membrane potential. Error bars represent SEM.

Figure 4. Inhibition of heat-activated TRPV3 currents by dyclonine.

(**A**) Sensitization of TRPV3 by heat. Heat-evoked TRPV3 currents in response to repeated temperature jumps. Temperature pulse generated by infrared laser diode irridation was stepped from room temperature to 51 ^{o}C in 1.5 ms and then clamped for 100 ms. (**B**) Effects of dyclonine on heat-activated TRPV3 currents. Heat-evoked current traces were recorded in whole-cell configuration, which were stabilized by sensitization of repeated fast temperature jumps as shown in (A). Temperature jumps shown on the top had a duration of 100 ms and a rise time of 1.5 ms. Bath solution with 0 or 30 μM dyclonine was applied by brief perfusion to the patch just before

temperature stimulation on the same cells. (**C**) The average plot compares the temperature responses in the absence and presence of 30 μM dyclonine (*Left*, $n = 6$). Currents were normalized by their maximum responses under control condition, respectively. Note that data from control and washout are superimposed. Percentage block of heat-evoked TRPV3 currents by 30 μM dyclonine as a function of temperature is shown on the right. (**D**) Representative inward currents evoked by a series of identical temperature jumps inhibited by dyclonine in a concentration-dependent manner. The temperature pulse (52 °C) is shown in gray. Holding potential was -60 mV. (**E**) Dose dependence of dyclonine effects on heat-activated TRPV3 currents. The solid line represents a fit to Hill's equation with $IC_{50} = 14.1 \pm 2.5$ μM and $n_H = 1.9 \pm 0.54$ ($n = 10$). All whole-cell recordings were got from TRPV3-expressing HEK 293T cells held at -60 mV.

Figure 5. Dyclonine rescued cell death caused by expression of overactive TRPV3 mutant.

(**A**-**B**) Effects of dyclonine on whole-cell currents recorded from TRPV3(G573S) and TRPV3(G573C) expressed in T-Rex 293 cells, showing that dyclonine (3 and 10 μM) reversibly inhibited the response to 300 μM 2-APB and the spontaneous activities at -60 mV. 20 μM RR was applied for subtracting leak currents. Bars represent duration of drug application. (**C**) Averaged inhibition of spontaneous activities of G573 mutants by dyclonine and RR. (**D**) Summary of relative whole-cell currents of

TRPV3(WT), G573S and G573S with or without dyclonine treatment. Error bars represent SEM. (**E**) Bright field and fluorescence images showing the cell survival. The GFP-tagged TRPV3 (wild-type, WT) and two mutants (G573C and G573S) in pcDNA4/TO vector were respectively transfected into T-Rex 293 cells, and then treated with doxycycline (20 ng/ml) for 16 h post-transfection to induce gene expression in the presence of drugs as indicated. Images of cells were taken at 12 h after induction. Scale bar, 50 μm. (**F**) Flow cytometry analysis of the percentage of dead cells. Cells transfected with the desired plasmids are as indicated. After the gene expression induced by doxycycline, the cells were treated with dyclonine (Dyc, 50 μM), 2-APB (30 μM), ruthenium red (RR, 10 μM) or the combination of 2-APB and dyclonine, and then stained with propidium iodide, followed by flow cytometry to analyze cell survival. (**G**) Summary plots of cell death rates under different treatments. Data were averaged from seven independent experiments. *** $P < 0.0001$.

Figure 6 Dyclonine suppresses scratching behavior induced by carvacrol.

(A) Summary of the time courses of neck-scratching behaviors in wild-type TRPV3 and TRPV3 knock out (C57BL/6) mice after intradermal injection of 50 μl carvacrol (0.1%) or normal saline (0.9% NaCl) containing 0.1% ethanol into the mouse neck. Time for scratching bouts was plotted for each five-minute interval over the 30 minutes observation period. (**B**) Quantification of the cumulative scratching bouts over 30 minutes under different treatments, showing that intradermal injection of carvacrol elicited a remarkable increase in the number of scratching bouts in

TRPV3$^{+/+}$ but not TRPV3$^{-/-}$ mice. (n = 6; N.S., no significance; *P < 0.05; **P < 0.01; ***P < 0.001, by one way ANOVA). (**C**) Time courses of neck-scratching behaviors in response to intradermal injection of 50 μl carvacrol (0.1%), with pretreatment of normal saline (0.9% NaCl), or different concentrations (1, 10, 50 μM) of dyclonine in the same site. (**D**) Summary plots of the number of scratching bouts over 30 minutes under different treatments as indicated, showing that dyclonine dose-dependently alleviated carvacrol-evoked acute itch. (n = 6; N.S., no significance; *P < 0.05; **P < 0.01; ***P < 0.001, by one way ANOVA). (**E**) Inhibition of carvacrol-evoked currents by dyclonine (Dyc) in a representative HEK 293T cell expressing TRPV3. After sensitization by repeated application of 300 μM 2-APB, the cell was exposed to 3, 30 or 50 μM dyclonine with 500 μM Carvacrol as indicated by the bars. Membrane currents were recorded in a whole-cell configuration, and the holding potential was -60 mV. (**F**) The dose-response curve for dyclonine inhibition of carvacrol-evoked TRPV3 currents was fitted by Hill's equation (IC_{50} = 3.5 ± 0.34 μM and n_H = 2.1 ± 0.41, n = 8).

Figure 7. Effects of dyclonine on single channel properties of TRPV3.

(**A**) Single-channel currents of TRPV3 were recorded from inside-out membrane patches of HEK 293T cells at two membrane potentials (±60 mV) in symmetrical 150 mM NaCl and were low-pass filtered at 2 kHz. Currents were evoked by 10 μM 2-APB in the absence and presence of dyclonine (30 μM) after sensitization induced by repetitive 300 μM 2-APB. All-point amplitude histograms of single-channel

973 currents were shown below the current traces. The histograms were fit to sums of two
974 Gaussian functions to determine the average amplitudes of currents and the open
975 probabilities. Dotted lines indicate the opened channel state (O) and the closed
976 channel state (C), respectively. (**B**) Summary of effects of dyclonine on TRPV3
977 single-channel open probability. Dyclonine (30 μM) decreased TRPV3 open
978 probability from 0.8 ± 0.02 to 0.08 ± 0.01 at -60 mV (n = 6), and from 0.82 ± 0.02 to
979 0.12 ± 0.01 at +60 mV (n =6), respectively. (**C**) I-V relationships of TRPV3
980 single-channel current evoked by 10 μM 2-APB without (black triangles) and with 30
981 μM dyclonine (red circles). Unitary conductance measured by fitting a linear function
982 were 163.6 ± 6.4 pS and 179.2 ± 5.5 pS for before and after treatment by dyclonine,
983 respectively.

984

985 **Figure 8. Molecular residues involved in dyclonine-TRPV3 interaction.**

986 (**A**) Overall view of the mTRPV3-dyclonine complex. Three putative binding modes
987 (BM) for dyclonine in the pore cavity of mTRPV3 channel (PDB ID code: 6DVZ) are
988 denoted as BM_A , BM_B and BM_C (please find the details in the text), with the
989 expanded view of BM_A shown on the right. Four subunits of the tetramer are
990 distinguished by different colors, and dyclonine in a schematic structure is shown in
991 red. (**B**) *Left*: potential docking poses of dyclonine and TRPV3 channel. *Right*: cluster
992 analysis showing all binding modes distributed into 3 clusters, BM_A, BM_B and BM_C.
993 (**C**) Representative whole-cell recordings show reversible blocking of 2-APB (1

994 mM)-evoked responses by dyclonine (3, 10 or 30 μM) in HEK 293T cells expressing
995 mutant TRPV3 channels as indicated, respectively. The combination of 3, 10 or 30
996 μM dyclonine and 2-APB was applied following the control currents evoked by a
997 saturated concentration of 2-APB (1 mM, initial grey bar). Holding potential was -60
998 mV. Bars represent duration of stimuli. (**D**) Concentration-response curves of
999 dyclonine on inhibition of the TRPV3 mutants. Solid lines represent fits by a Hill
1000 equation, with the half-maximal inhibitory concentration (IC_{50}) shown in (**E**). For
1001 comparison, the dose-response curve of wile-type channel is displayed in gray. Four
1002 point mutations (L630W, N643A, I644W and L655A) reduced the inhibitory
1003 efficiency of dyclonine, while the other two point mutations (L642A and I659A)
1004 enhanced the inhibitory effects of dyclonine on TRPV3 currents. (**F**) Average current
1005 responses of mutant channels compared with wild-type TRPV3 channels. Each
1006 substitution of putative residues except L639A retained their normal responses to
1007 2-APB. Numbers of cells are indicated in parentheses. (**G**) Modulation of
1008 thiol-oxidizing and disulfide-reducing agents on the inhibitory effects of dyclonine.
1009 Whole-cell recordings from the wild-type TRPV3 and the mutants expressed in HEK
1010 293T cells, showing the effects of MTSET and DTT on the responses to 2-APB with
1011 or without dyclonine after sensitization induced by 300 μM 2-APB. MTSET (1 mM)
1012 and DTT (10 mM) were locally applied for ~3 min to probe the accessibility,
1013 respectively. The responsiveness to 2-APB or 2-APB plus dyclonine was subsequently
1014 examined before and after treatments. Holding potential was -60 mV. (**H**) Summary of
1015 inhibition of relative currents elicited by 300 μM 2-APB, 300 μM 2-APB with

dyclonine 10 or 1 μM. (**I**) Summary of inhibitory effects of dyclonine before and after treatments with MTSET and DTT. The dotted line indicates zero current level in all cases. Error bar represents SEM. N.S., no significance; *$P < 0.05$; **$P < 0.01$; ***$P < 0.001$.

Figure 6—figure Supplement 1. Effects of dyclonine on the excitability of mouse DRG and TG neurons as well as the TRPV3-mediated nociceptive behavior.

(A-B) Current-clamp responses of DRG and TG neurons to 500 ms current pulse injection, respectively. Protocol of injected current is shown on the top. (**C**) Statistics plot showing no significant changes for RMP (resting membrane potential) from DRG or TG neurons in the presence of dyclonine (10 μM) compared with control. RMP were -44 ± 1.3 mV (n = 5) vs. -45 ± 0.9 mV (n = 5) treated with dyclonine in DRG neurons, and -44.8 ± 1.3 mV (n = 5) vs. -47.2 ± 1.9 mV (n = 5) treated with dyclonine in TG neurons. (**D**) Comparison of averaged frequency of action potential (AP) firing (numbers of action potential firing) evoked by current injection of 125 pA lasting for 500 ms in DRG and TG neurons. (**E**) Paw withdrawal or licking latencies to noxious thermal stimuli at 55 °C evaluating the effect of dyclonine on thermal pain sensing. The paw withdrawal latencies (PWL) were 16.57 ± 0.46 s (n = 12), 18.08 ± 0.03 s (n = 12) and 18.82 ± 0.42 s (n = 12) for hind paws with intraplantar injection with saline, 10 μM and 50 μM dyclonine in *TRPV3*$^{+/+}$ mice, respectively. The PWL were 18.93 ± 0.61 s (n = 12), 18.23 ± 0.52 s (n = 12), and 18.61 ± 0.46 s (n = 12) for hind paws

with intraplantar injection with saline, 10 μM and 50 μM dyclonine in *TRPV3*$^{-/-}$ mice. N.S., no significance; *$P < 0.05$; **$P < 0.01$; ***$P < 0.001$.

Figure 8—figure supplement 1. **Residues in the TRPV3 channel pore for interacting with dyclonine.**

(**A**) Receptor grid for docking generated with 35 Å × 35 Å × 35 Å dimensions. (**B**) Detailed binding modes of dyclonine in BM_B and BM_C. The putative interaction residues are labeled and dyclonine is displayed in sticks for emphasis. (**C**) Representative whole-cell recordings show reversible blocking of 2-APB (1 mM)-evoked responses by dyclonine (10 or 30 μM) in HEK 293T cells expressing mutant TRPV3 channels as indicated, respectively. Holding potential was -60 mV. Bars represent duration of stimuli. (**D**) Concentration-response curves of dyclonine on inhibition of the TRPV3 mutants. Solid lines represent fits by a Hill equation, with the half-maximal inhibitory concentration (IC_{50}) shown in (**E**). For comparison, the dose-response curve of wild-type is displayed in gray. (**F**) Average current responses of mutant channels compared with wild-type TRPV3 channels. Only cells that expressed I637A, F666A or I674A showed similar response as wild-type channel, while others with the substation by alanine were not functional. Numbers of cells are indicated in parentheses. (**G**) Structures assigned to apo/resting (left) and open states (right). (**H**) Cavity fostered by the pore helix and S5-S6 domains of TRPV3 channels at the resting (left) and open (right) states.

Figure 8—figure supplement 2. Alignment of the pore-region sequences.

Alignment of the pore sequence of mTRPV3 with other TRP channels, with the identical or similar residues shaded in colors. Meanwhile, differences in amino acids compositions present for different channels. The key residues of TPRV3 are indicated at the top, which affects the inhibitory effect of dyclonine.

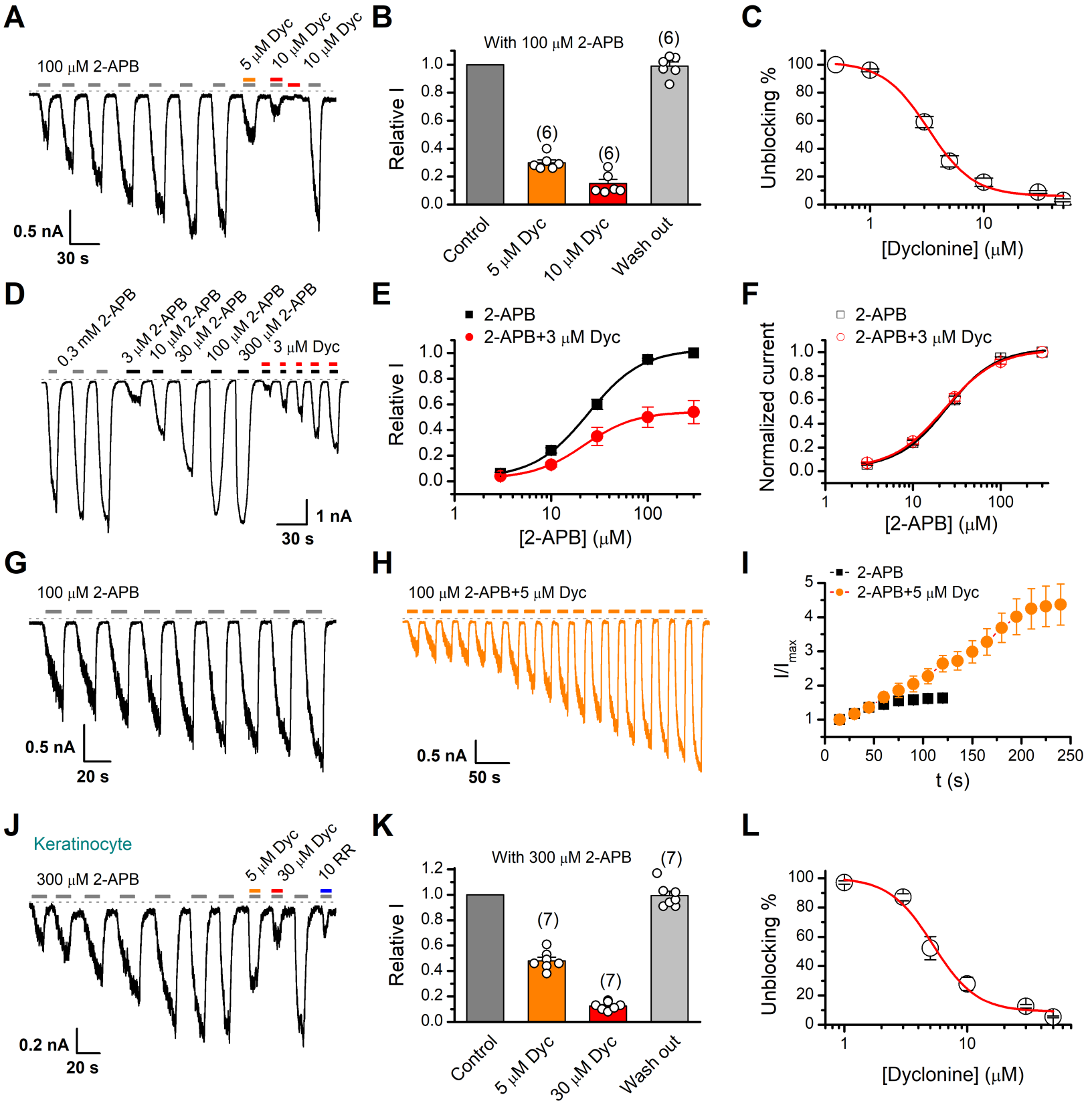
A
100 μM 2-APB
5 μM Dyc
10 μM Dyc
10 μM Dyc
0.5 nA
30 s
B
With 100 μM 2-APB
Relative I
(6)
(6)
(6)
Control
5 μM Dyc
10 μM Dyc
Wash out
C
Unblocking %
[Dyclonine] (μM)
D
0.3 mM 2-APB
3 μM 2-APB
10 μM 2-APB
30 μM 2-APB
100 μM 2-APB
300 μM 2-APB
3 μM Dyc
1 nA
30 s
E
2-APB
2-APB+3 μM Dyc
Relative I
[2-APB] (μM)
F
2-APB
2-APB+3 μM Dyc
Normalized current
[2-APB] (μM)
G
100 μM 2-APB
0.5 nA
20 s
H
100 μM 2-APB+5 μM Dyc
0.5 nA
50 s
I
2-APB
2-APB+5 μM Dyc
I/I_max
t (s)
J
Keratinocyte
300 μM 2-APB
5 μM Dyc
30 μM Dyc
10 RR
0.2 nA
20 s
K
With 300 μM 2-APB
Relative I
(7)
(7)
(7)
Control
5 μM Dyc
30 μM Dyc
Wash out
L
Unblocking %
[Dyclonine] (μM)

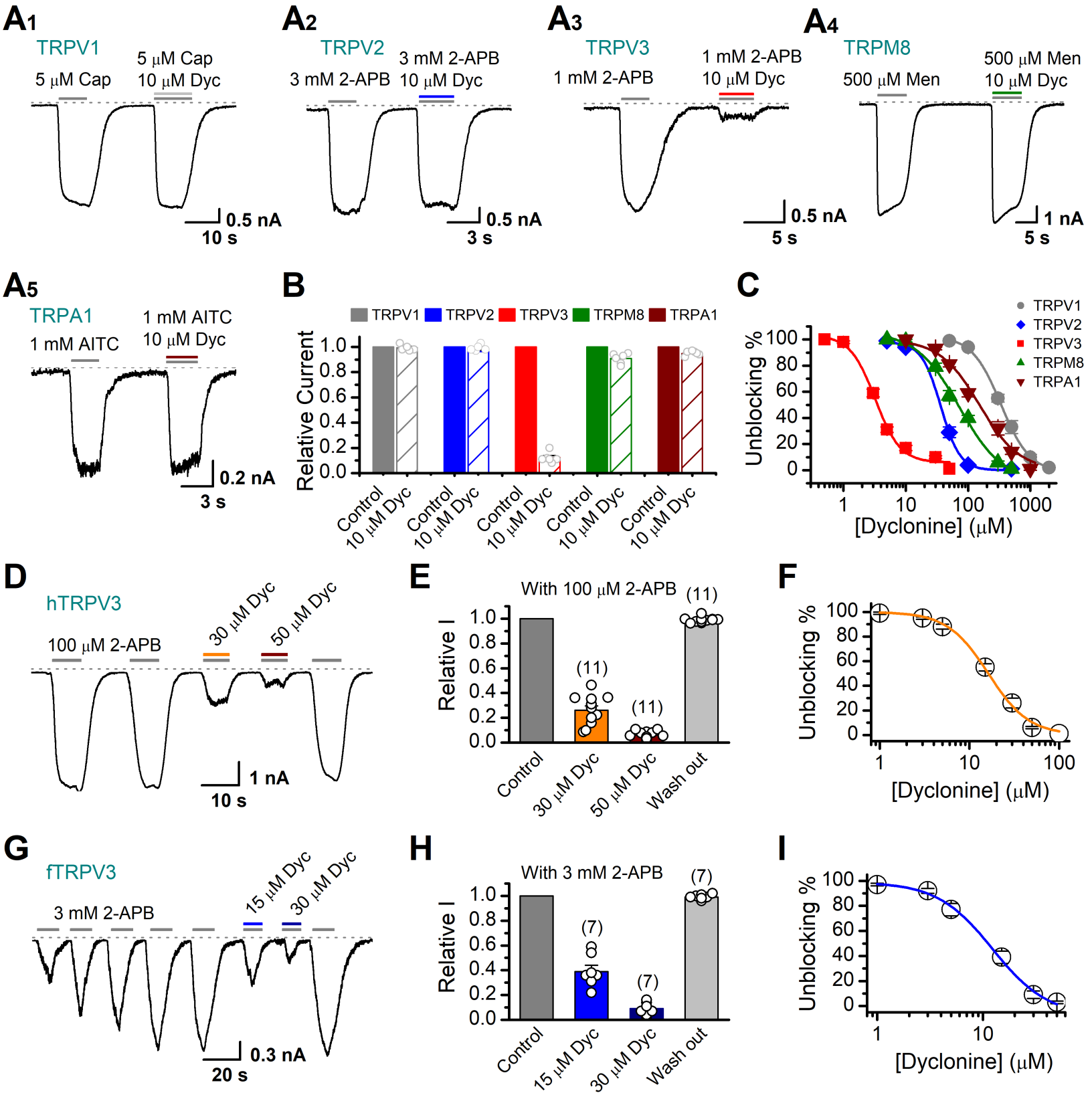
A1
TRPV1
5 μM Cap
5 μM Cap
10 μM Dyc
0.5 nA
10 s
A2
TRPV2
3 mM 2-APB
3 mM 2-APB
10 μM Dyc
0.5 nA
3 s
A3
TRPV3
1 mM 2-APB
1 mM 2-APB
10 μM Dyc
0.5 nA
5 s
A4
TRPM8
500 μM Men
500 μM Men
10 μM Dyc
1 nA
5 s
A5
TRPA1
1 mM AITC
1 mM AITC
10 μM Dyc
0.2 nA
3 s
B
TRPV1 TRPV2 TRPV3 TRPM8 TRPA1
Relative Current
Control
10 μM Dyc
C
TRPV1
TRPV2
TRPV3
TRPM8
TRPA1
Unblocking %
[Dyclonine] (μM)
D
hTRPV3
100 μM 2-APB
30 μM Dyc
50 μM Dyc
1 nA
10 s
E
With 100 μM 2-APB
(11)
Relative I
Control
30 μM Dyc
50 μM Dyc
Wash out
F
Unblocking %
[Dyclonine] (μM)
G
fTRPV3
3 mM 2-APB
15 μM Dyc
30 μM Dyc
0.3 nA
20 s
H
With 3 mM 2-APB
(7)
Relative I
Control
15 μM Dyc
30 μM Dyc
Wash out
I
Unblocking %
[Dyclonine] (μM)

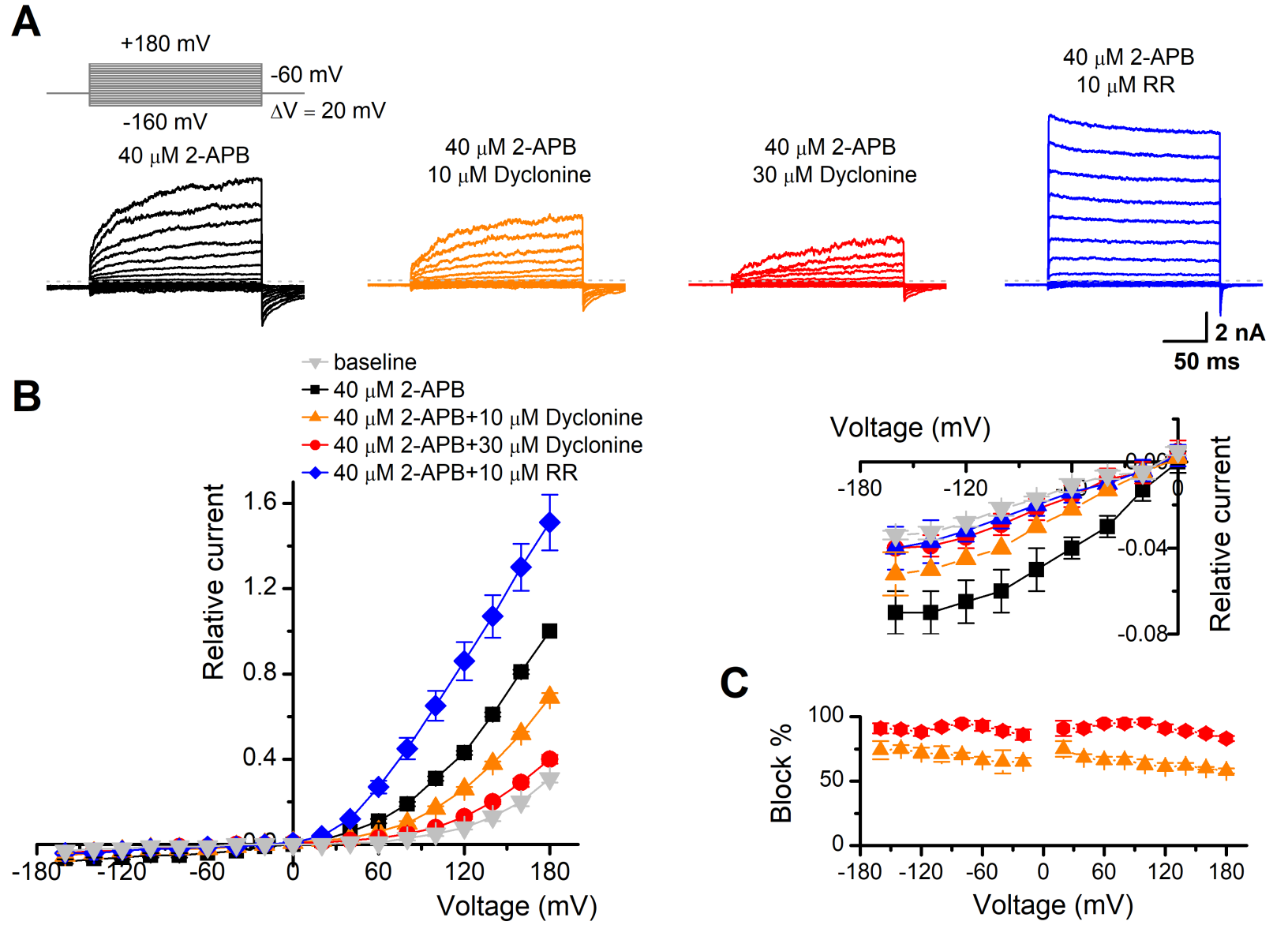
A
+180 mV
-60 mV
ΔV = 20 mV
-160 mV
40 μM 2-APB
40 μM 2-APB
10 μM Dyclonine
40 μM 2-APB
30 μM Dyclonine
40 μM 2-APB
10 μM RR
2 nA
50 ms
B
baseline
40 μM 2-APB
40 μM 2-APB+10 μM Dyclonine
40 μM 2-APB+30 μM Dyclonine
40 μM 2-APB+10 μM RR
Relative current
Voltage (mV)
C
Block %
Voltage (mV)

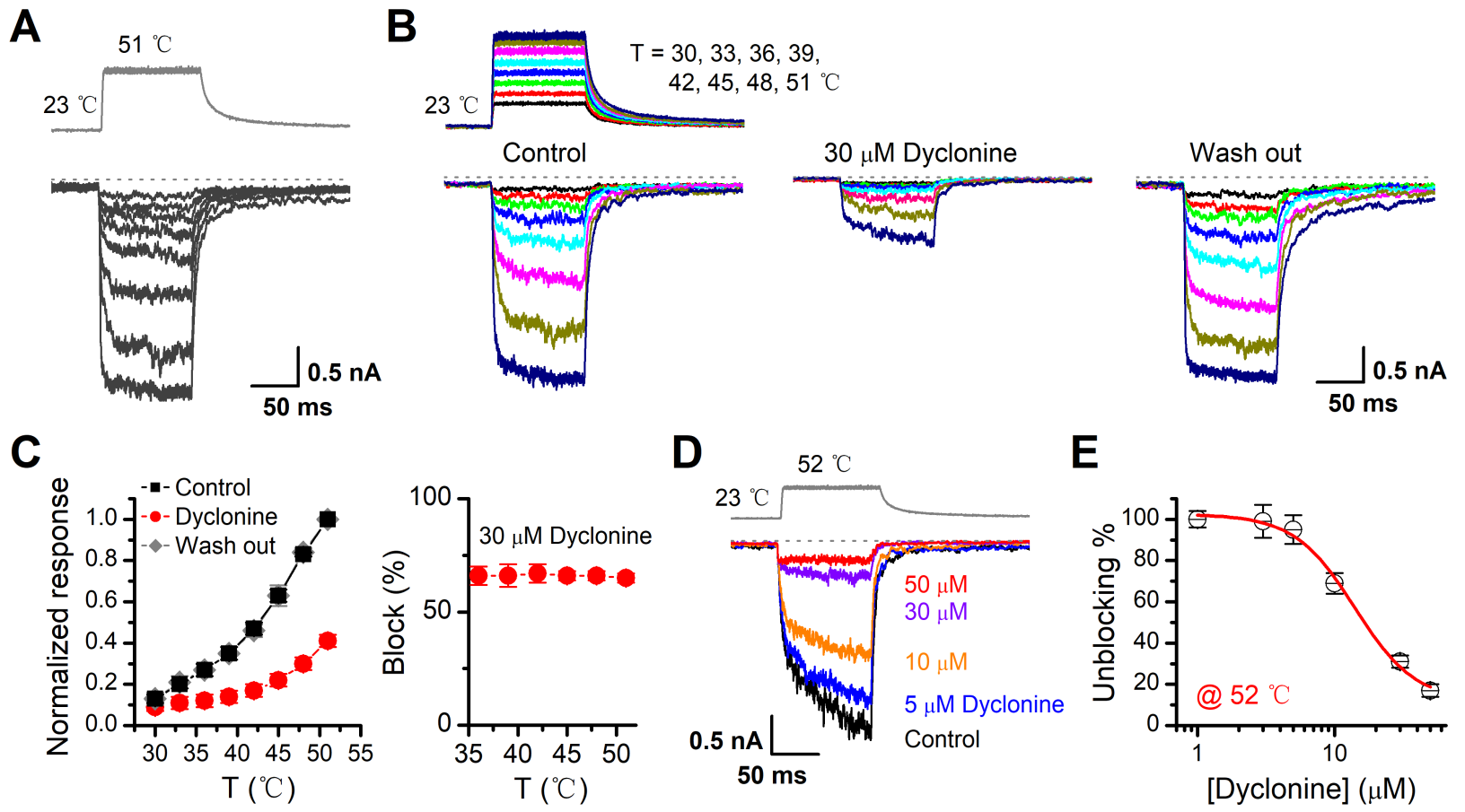
A
51 ℃
23 ℃
0.5 nA
50 ms
B
T = 30, 33, 36, 39,
42, 45, 48, 51 ℃
23 ℃
Control
30 μM Dyclonine
Wash out
0.5 nA
50 ms
C
Control
Dyclonine
Wash out
Normalized response
T (℃)
30 μM Dyclonine
Block (%)
T (℃)
D
52 ℃
23 ℃
50 μM
30 μM
10 μM
5 μM Dyclonine
Control
0.5 nA
50 ms
E
Unblocking %
@ 52 ℃
[Dyclonine] (μM)

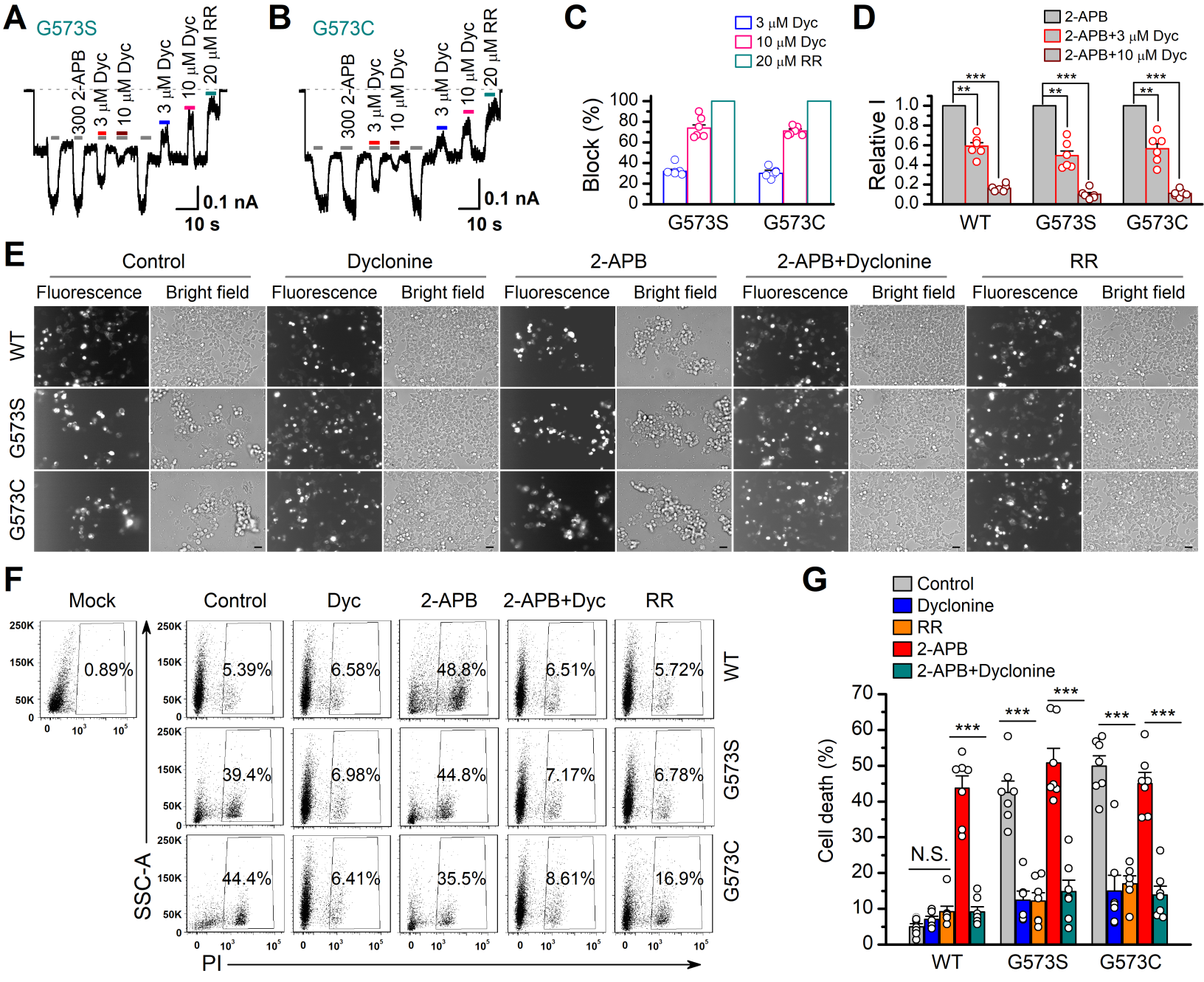
A
G573S
300 2-APB
3 μM Dyc
10 μM Dyc
3 μM Dyc
10 μM Dyc
20 μM RR
0.1 nA
10 s
B
G573C
300 2-APB
3 μM Dyc
10 μM Dyc
3 μM Dyc
10 μM Dyc
20 μM RR
0.1 nA
10 s
C
3 μM Dyc
10 μM Dyc
20 μM RR
Block (%)
100
80
60
40
20
0
G573S
G573C
D
2-APB
2-APB+3 μM Dyc
2-APB+10 μM Dyc
Relative I
1.0
0.8
0.6
0.4
0.2
0.0
***
**
WT
G573S
G573C
E
Control
Dyclonine
2-APB
2-APB+Dyclonine
RR
Fluorescence
Bright field
WT
G573S
G573C
F
Mock
Control
Dyc
2-APB
2-APB+Dyc
RR
0.89%
5.39%
6.58%
48.8%
6.51%
5.72%
39.4%
6.98%
44.8%
7.17%
6.78%
44.4%
6.41%
35.5%
8.61%
16.9%
WT
G573S
G573C
SSC-A
PI
G
Control
Dyclonine
RR
2-APB
2-APB+Dyclonine
Cell death (%)
N.S.
***
WT
G573S
G573C

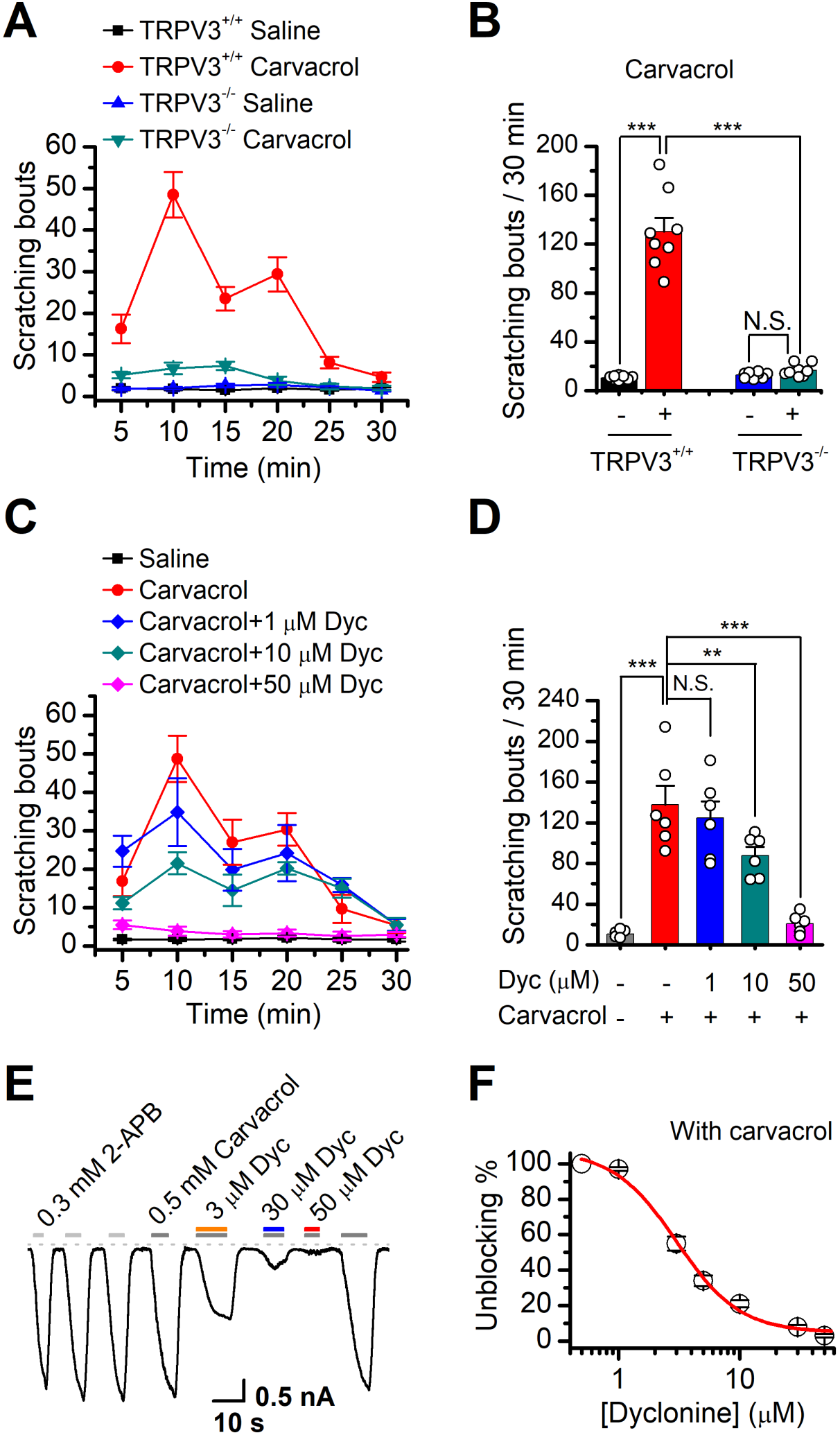
A
TRPV3+/+ Saline
TRPV3+/+ Carvacrol
TRPV3-/- Saline
TRPV3-/- Carvacrol
Scratching bouts
Time (min)
B
Carvacrol
Scratching bouts / 30 min
***
***
N.S.
TRPV3+/+
TRPV3-/-
C
Saline
Carvacrol
Carvacrol+1 μM Dyc
Carvacrol+10 μM Dyc
Carvacrol+50 μM Dyc
Scratching bouts
Time (min)
D
Scratching bouts / 30 min
***
**
N.S.
***
Dyc (μM)
Carvacrol
E
0.3 mM 2-APB
0.5 mM Carvacrol
3 μM Dyc
30 μM Dyc
50 μM Dyc
0.5 nA
10 s
F
With carvacrol
Unblocking %
[Dyclonine] (μM)

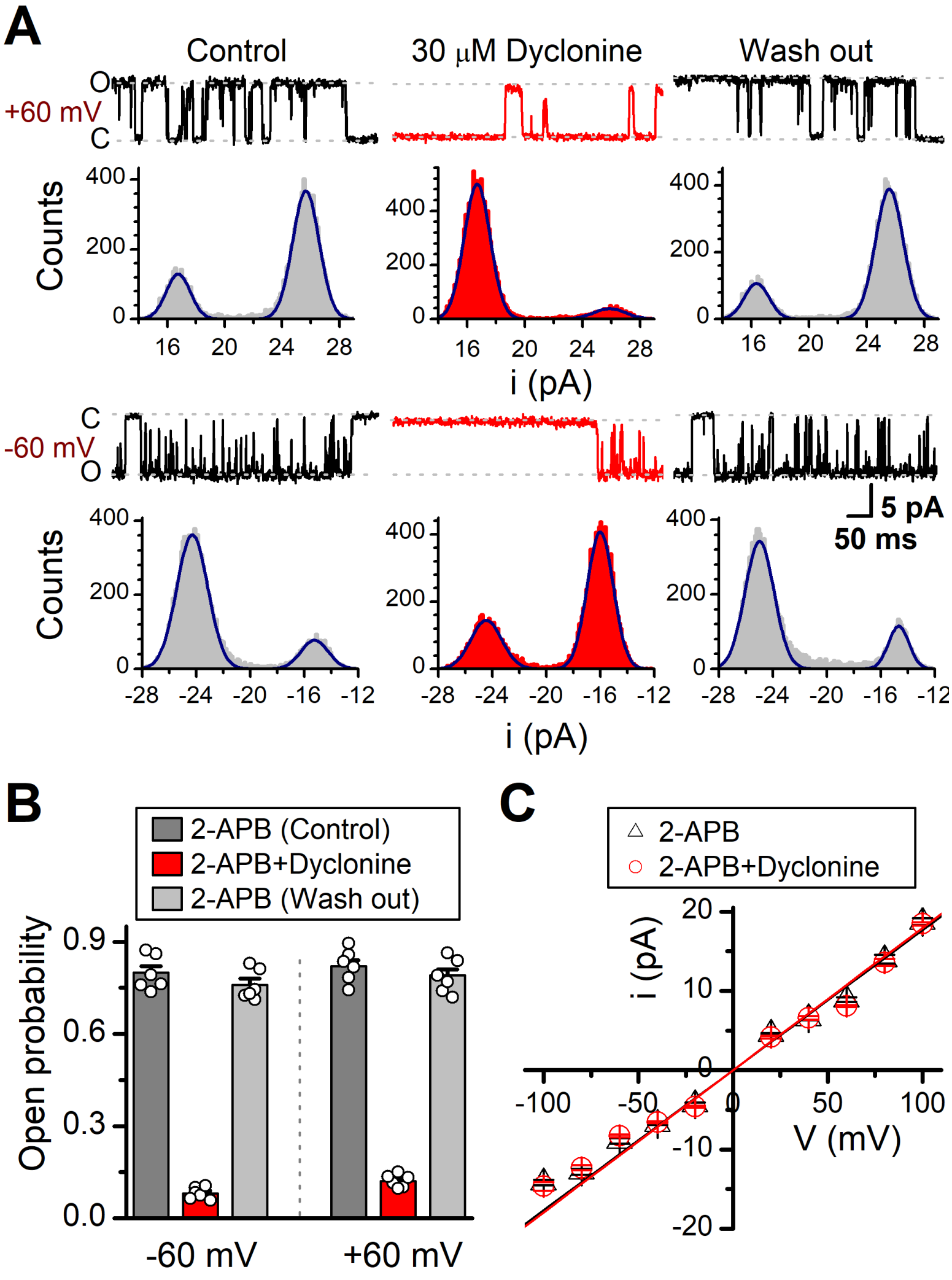
A
Control
30 μM Dyclonine
Wash out
+60 mV
O
C
Counts
400
200
0
16
20
24
28
i (pA)
-60 mV
C
O
5 pA
50 ms
-28
-24
-20
-16
-12
B
2-APB (Control)
2-APB+Dyclonine
2-APB (Wash out)
Open probability
0.9
0.6
0.3
0.0
-60 mV
+60 mV
C
2-APB
2-APB+Dyclonine
i (pA)
20
10
0
-10
-20
-100
-50
50
100
V (mV)

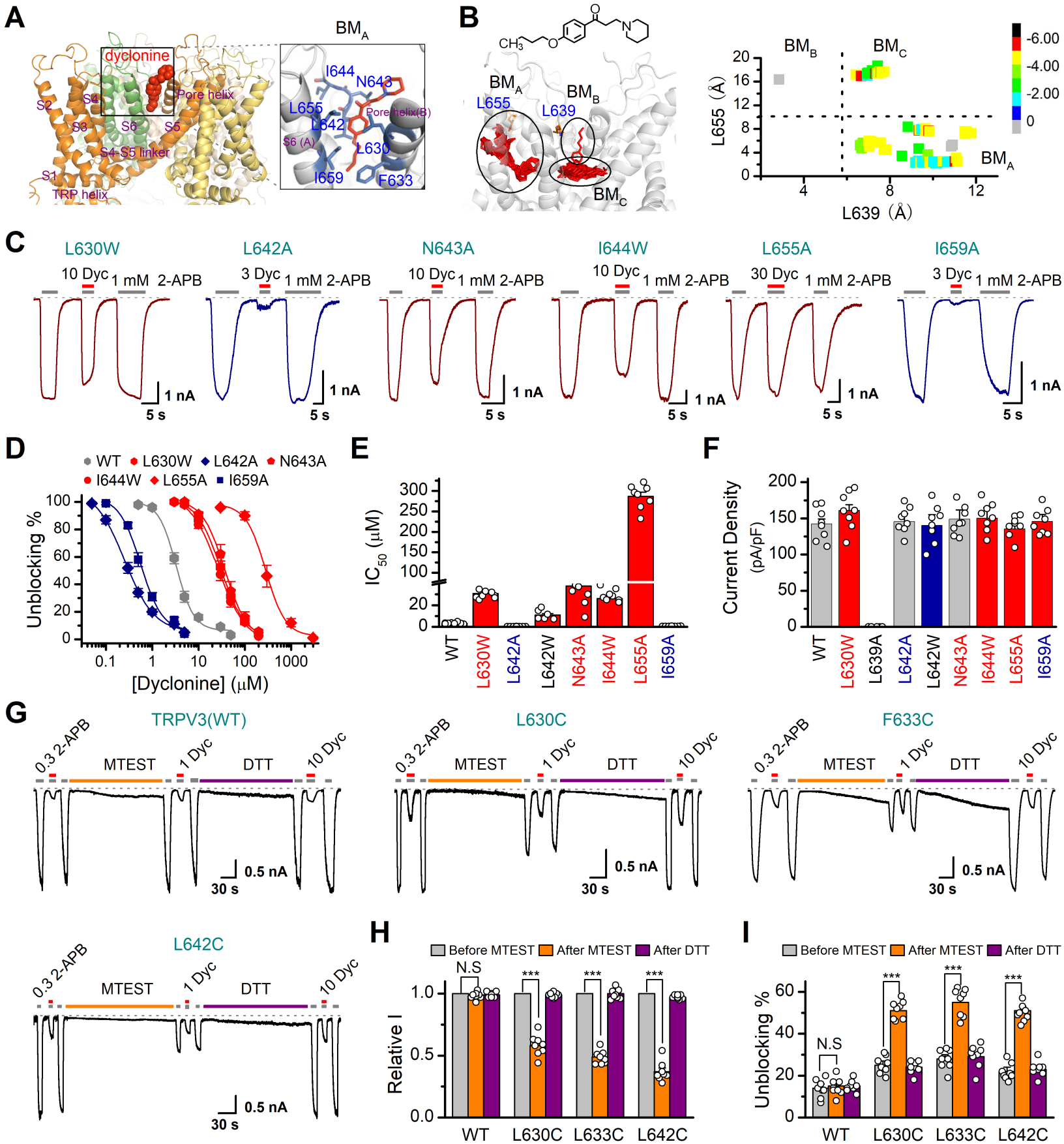
A
dyclonine
S2
S4
S3
S6
S5
Pore helix
S4-S5 linker
S1
TRP helix
BM_A
I644
N643
L655
L642
Pore helix(B)
S6 (A)
L630
I659
F633
B
CH3
O
N
BM_A
BM_B
L655
L639
BM_C
BM_B
BM_C
BM_A
L655 (Å)
L639 (Å)
-6.00
-4.00
-2.00
0
C
L630W
10 Dyc
1 mM 2-APB
L642A
3 Dyc
N643A
10 Dyc
I644W
10 Dyc
L655A
30 Dyc
I659A
3 Dyc
1 nA
5 s
D
WT
L630W
L642A
N643A
I644W
L655A
I659A
Unblocking %
[Dyclonine] (μM)
E
IC50 (μM)
WT
L630W
L642A
L642W
N643A
I644W
L655A
I659A
F
Current Density
(pA/pF)
WT
L630W
L639A
L642A
L642W
N643A
I644W
L655A
I659A
G
TRPV3(WT)
L630C
F633C
L642C
0.3 2-APB
MTEST
1 Dyc
DTT
10 Dyc
0.5 nA
30 s
H
Before MTEST
After MTEST
After DTT
N.S
***
Relative I
WT
L630C
L633C
L642C
I
Unblocking %
N.S
***
WT
L630C
L633C
L642C

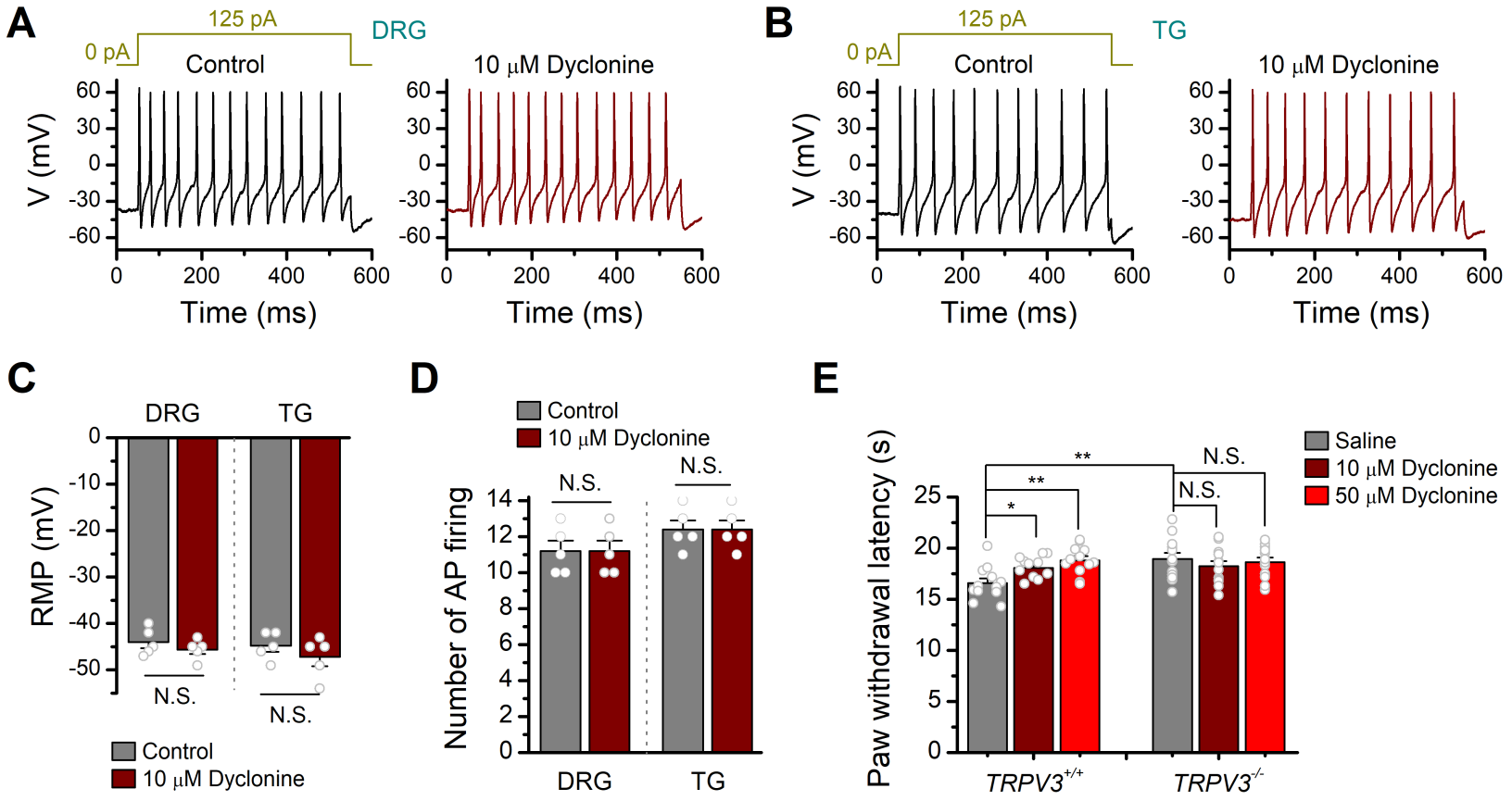
A
125 pA
0 pA
DRG
Control
10 μM Dyclonine
V (mV)
Time (ms)
B
125 pA
0 pA
TG
Control
10 μM Dyclonine
V (mV)
Time (ms)
C
DRG
TG
RMP (mV)
N.S.
N.S.
Control
10 μM Dyclonine
D
Control
10 μM Dyclonine
Number of AP firing
N.S.
N.S.
DRG
TG
E
Saline
10 μM Dyclonine
50 μM Dyclonine
Paw withdrawal latency (s)
*
**
**
N.S.
N.S.
TRPV3+/+
TRPV3-/-

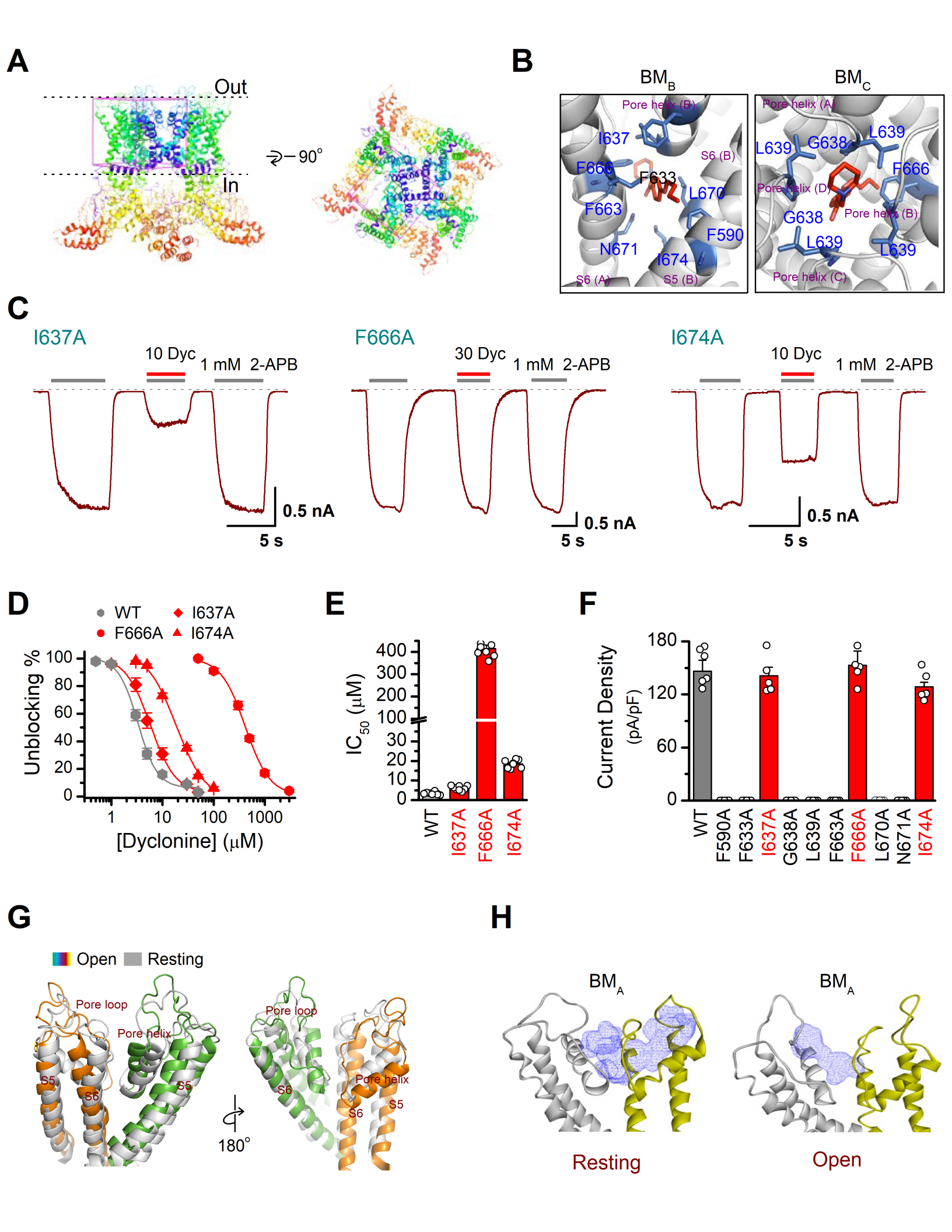
A
Out
In
90°
B
BM_B
Pore helix (B)
I637
S6 (B)
F666
F633
L670
F663
F590
N671
I674
S6 (A)
S5 (B)
BM_C
Pore helix (A)
L639
G638
L639
F666
Pore helix (D)
Pore helix (B)
G638
L639
L639
Pore helix (C)
C
I637A
10 Dyc
1 mM 2-APB
0.5 nA
5 s
F666A
30 Dyc
1 mM 2-APB
0.5 nA
5 s
I674A
10 Dyc
1 mM 2-APB
0.5 nA
5 s
D
WT
I637A
F666A
I674A
Unblocking %
100
80
60
40
20
0
1
10
100
1000
[Dyclonine] (μM)
E
IC50 (μM)
400
300
200
100
30
20
10
0
WT
I637A
F666A
I674A
F
Current Density (pA/pF)
180
120
60
0
WT
F590A
F633A
I637A
G638A
L639A
F663A
F666A
L670A
N671A
I674A
G
Open
Resting
Pore loop
Pore helix
S5
S6
S5
180°
Pore loop
S6
Pore helix
S6
S5
H
BM_A
BM_A
Resting
Open

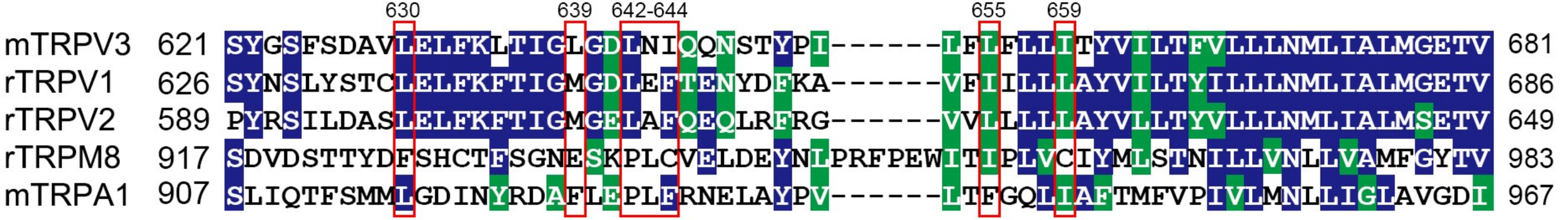
630
639
642-644
655
659
mTRPV3 621 SYGSFSDAVLELFKLTIGLGDLNIQQNSTYPI------LFLFLLITYVILTFVLLLNMLIALMGETV 681
rTRPV1 626 SYNSLYSTCLELFKFTIGMGDLEFTENYDFKA------VFIILLLAYVILTYILLLNMLIALMGETV 686
rTRPV2 589 PYRSILDASLELFKFTIGMGELAFQEQLRFRG------VVLLLLLAYVLLTYVLLLNMLIALMSETV 649
rTRPM8 917 SDVDSTTYDFSHCTFSGNESKPLCVELDEYNLPRFPEWITIPLVCIYMLSTNILLVNLLVAMFGYTV 983
mTRPA1 907 SLIQTFSMMLGDINYRDAFLEPLFRNELAYPV------LTFGQLIAFTMFVPIVLMNLLIGLAVGDI 967